Hardness Characteristics in Electrodeposited Cu/Ni Multilayer Systems

By

Li Zhaojiang

A Thesis
Submitted to the College of Graduate Studies and Research
through the Department of Physics in the partial
Fulfillment of the Requirements for the
Degree of master of Science at
the University of Windsor
Windsor, Ontario
1999

©1999, Li Zhaojiang

National Library of Canada
Acquisitions and Bibliographic Services
395 Wellington Street
Ottawa ON K1A 0N4
Canada

Bibliothèque nationale du Canada
Acquisitions et services bibliographiques
395, rue Wellington
Ottawa ON K1A 0N4
Canada

Your file Votre référence

Our file Notre référence

The author has granted a non-exclusive licence allowing the National Library of Canada to reproduce, loan, distribute or sell copies of this thesis in microform, paper or electronic formats.

The author retains ownership of the copyright in this thesis. Neither the thesis nor substantial extracts from it may be printed or otherwise reproduced without the author's permission.

L'auteur a accordé une licence non exclusive permettant à la Bibliothèque nationale du Canada de reproduire, prêter, distribuer ou vendre des copies de cette thèse sous la forme de microfiche/film, de reproduction sur papier ou sur format électronique.

L'auteur conserve la propriété du droit d'auteur qui protège cette thèse. Ni la thèse ni des extraits substantiels de celle-ci ne doivent être imprimés ou autrement reproduits sans son autorisation.

0-612-52687-9

Canada

Abstract

Multilayered Cu/Ni thin films were grown epitaxially on copper substrate using electrodeposition method. The multilayers possess coherent interfaces with well-defined satellites surrounding the main Bragg peaks in the X-Ray diffractograms. Hardness values greater than those of the constituent materials, by a factor of two or better, were found. Also, a Hall-Petch type relationship between hardness and superlattice periodicity, that is, hardness is in proportion to the inverse of the square root of the superlattice periodicity, is determined for superlattice periodicity in the range of about 40 to 80 angstroms. When nickel thickness is fixed at about 50 angstroms, hardness is independent of copper thickness for the range of from 16 to 32 angstroms. On the other hand, hardness drops when nickel thickness increases from about 17 to 41 angstroms while copper thickness is fixed at about 10 angstroms,.

Dedication

This thesis is dedicated to my mother Liu Ruilan and my father Li Chuanqiu.

Acknowledgement

The author would like to express his appreciation to John Roberts and Johnathan Farr for their assistance in carrying out the X-Ray diffraction experiments and the hardness measurement. Dr. D. D. Synder's arrangement for the part of work at GM is greatly appreciated.

The author would also like to thank his colleagues Tim Rausch and Dr. T. Szczurek for their cooperation in the project.

Last but not least, the guidance and encouragement from Dr. M. Schlesinger throughout this project is gratefully acknowledged.

Contents

Abstract iii

Dedication iv

Acknowledgement v

Chapter 1: Introduction 1

Chapter 2: Theoretical background 7

2.1 Superlattice structure and growth of superlattices 7

2.1.1 Structural and chemical orders of superlattices 7

2.1.2 Mechanisms of superlattice growth 9

2.1.3 Formation of the orientation of superlattices 13

2.2 Electrochemistry 18

2.2.1 Fundamental equation for an electrochemical cell 18

2.2.2 The electrochemical reactions in the Cu/Ni multilayer bath 24

2.3 X-Ray crystallography 30

2.3.1 Crystalline structure 30

2.3.2 Bragg's law 32

2.3.3 X-Ray diffraction in superlattices 34

2.4 Hardness characteristics of superlattices 36

Chapter 3: Experimental 51

3.1 Electrodeposition process 51

3.2 X-Ray investigation of samples 64

3.3 Hardness test 65

Chapter 4: Results 69

4.1 X-Ray diffractograms 69

4.2 Hardness results 73

Chapter 5: Discussions 82

5.1 X-Ray diffraction 82

5.2 Hardness results 83

Chapter 6: Conclusions 87

References 88

Vita Auctoris 90

Chapter 1

Introduction

The search for materials with unusual hardnesses has long been of considerable interest to human beings. Materials with high hardness have found many applications in industry and other sectors of human life. Many technological applications such as cutting, abrading, polishing and coating put a demand on materials with unusually high hardnesses. Some materials come naturally with super hardnesses, diamond[1], for example. They have already been put into use extensively. However, their reserve in nature is limited and their prices are prohibitive. Furthermore, these naturally-occurring hard materials have often exhibited properties unfavorable to conditions in certain applications. For instance, diamond burns in air at 700°C to form carbon dioxide[2], ruling it out for applications at high temperatures. Naturally, humans have sought to synthesize materials with appreciable hardnesses as an alternative.

There have been theoretical predictions[3] that a hypothetical crystal – the "hexagonal β form" of carbon nitride (C_3N_4) – would produce a bulk modulus (and hence presumably a hardness) similar or greater than that of diamond. However, many attempts to synthesize this material have failed[2].

On the other hand, superlattices, which are made up of alternating layers of different materials, have been successfully produced to yield hardnesses ranging from 30 Gpa to 50 Gpa[2]. As a comparison, diamond, the hardest material found in nature, has a hardness of about 80 to 100 Gpa. An improvement of hardness by a factor of 2.5 than

would be expected from the simple alloy of constituent materials is typical of a range of superlattice materials[1].

It was first suggested by James Koehler[4] in 1970 that high strength could be obtained from a composite material with alternating layers of different constituent materials of similar structures but significantly different elastic constants. Since then, interest has been growing in producing multilayered materials in which mechanical properties distinct from their bulk materials can be expected. A number of research workers have reported success in this regard[5]-[11].

William D. Sproul[6] and Dong Li[11] produced polycrystalline nitride (TiN/VN, TiN/NbN) superlattice coatings using magnetron sputtering system. The films possessed hardnesses exceeding 50 Gpa; B. J. Daniels[8] and others sputter-deposited epitaxial Fe(001)/Pt(001) multilayers on MgO(001), which exhibited hardnesses over that expected from a simple rule of mixture by a factor of 2.5; Cu/Ni multilayers, the most extensively studied superlattice system reported, have been produced using dual ion beam sputtering and electrodeposition respectively. They also displayed enhanced hardness over that of nickel and copper[5][12].

A few projects have been devoted to the study of hardness dependence on superlattice structure -- mostly the super lattice periodicity, that is, the repeat length Λ, of the bilayers -- as shown in Figure 1.1.

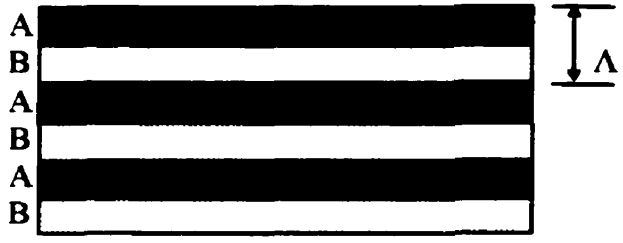

Figure 1.1: Schematic structure of a superlattice system with two alternating layers A and B. The repeat length Λ is called the superlattice periodicity or wavelength.

It is an established fact that superlattice hardness is a function of its periodicity, among other things. One of the widely used relationships regarding hardness dependence on superlattice periodicity is the Hall-Petch relation. It states that within a certain range of the periodicity values, hardness (H) varies in proportion to the inverse of the square root of the superlattice periodicity (Λ), $H \propto \Lambda^{-1/2}$. This has been confirmed in some experiments. R. C. Cammarata, et al. [7] claimed that when the superlattice periodicity is reduced to below 50 Angstroms, unusual elastic and plastic properties are observed and for dual-ion-beam-sputter-deposited Cu/Ni system a Hall-Petch type relation is found for periodicity values ranging from 20 to over 100 Angstroms; R. F. Bunshan, R. Nimmagadda and H. J. Doerr[13] reported a Hall-Petch type relationship in Cu/Ni system prepared with electron beam evaporation.

However, there have also been reports in the literature that put this conclusion in question. B. J. Daniels, W. D. Nix and B. M. Clemens found that their sputter-deposited Fe/Pt system possesses increased hardness over a considerable range in Λ (20 - 100 Angstroms) but is not a function of Λ[8].

It is reasonable to believe that hardness depends not only on the superlattice periodicity, but also on the thickness ratio of its constituent materials. Since little information was found in the literature on the latter topic it was included in the work of this thesis, among others.

There are also several different methods for measuring hardness, such as "Vickers hardness test" which uses a symmetric diamond tip and "Knoop test" using an asymmetric tip. These different methods often yield quite different results even on the same samples, thus compromising the credibility of some earlier claims regarding hardness characteristics[12]. The recently-developed "nano-indentation technique" which enables measurements to be made at very low forces is believed to be more suitable for thin film measurements and it was used in the work of this paper.

Several models have been established to explain the hardness enhancement mechanism of superlattice structures[1]. James Koehler's[4] model is by far the most successful one. He said that the interfaces between the layers would act as barriers to the motion of dislocations, which are the line defects that are mainly responsible for the plastic deformation of crystalline solids. Restricting the motion of dislocations in this way would strengthen this type of material. Xi Chu and Scott A. Barnett[14] improved this model recently by incorporating the fact that the interfaces in a superlattice are not perfectly abrupt. They pointed out that for miscible materials such as TiN/NbN, the interfaces between two adjacent layers can be at least 1 nm wide. Broader interfaces of this kind tend to reduce the effect of having alternate layers with different shear moduli. This new model better explains the quantitative dependence of hardness on superlattice periodicity.

For the enhanced hardness effect to occur, the multilayered structures must posses coherent interfaces. The coherency of the interfaces of the multilayers can be examined using X-ray diffraction[15][16]. A finely-structured multilayer exhibits both the main Bragg peak and satellites to both sides of the main peak as shown in Figure 1.2. There are a number of methods in existence for fabricating multilayers.

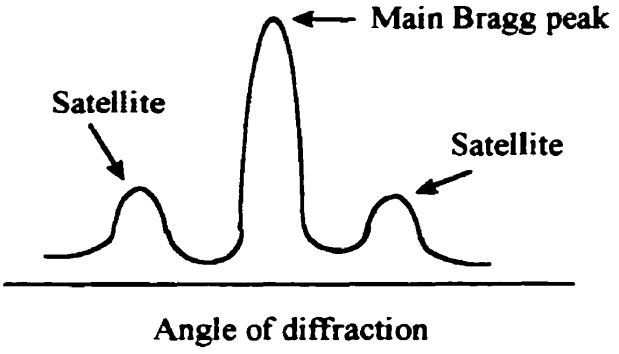

Figure 1.2: Schematic X-ray diffraction diagram of a well-structured superlattice

As mentioned earlier, most of the multilayer systems investigated for hardness characteristics were prepared by physical vapor deposition (PVD) methods such as electron beam evaporation (EBE) or dc magnetron sputtering.

As many properties of a superlattice depends on its preparation method, many of the conclusions drawn in these cases may not be applied to explain the properties of systems prepared by other methods, such as electrodeposition which is used in the work of this paper.

Each of the different methods for producing multilayers has its own advantages and disadvantages. The physical methods produce better quality (cleaner) samples because the source materials are placed separately in the vacuum chamber. But they require an

expensive ultrahigh vacuum system (~10^{-9} Torr) and deposition rate is slow[17]. Electrodeposition has been gaining more and more popularity in recent years and has found significant applications in making protective and decorative coatings. Electrodeposition[17], which will be detailed in Chapter 3, refers to the deposition of one or two kinds of materials (generally metal) from a bath containing a solution of the ions of the materials by the passage of an electric current. The nature of an electrodeposit is determined by many factors including the electrolyte composition, pH, temperature and agitation, the potentials applied between the electrodes, and the current density. It features low processing temperatures, high deposition rate, low cost and the possibility of tailoring the crystallographic texture and the composition of the deposit. The drawbacks of electrodeposition are the purity problem associated with a single-bath deposition, which can result in the damage of the multilayer systems in the post-production treatment and can also affect the properties of the multilayer systems.

The focus of the work in this paper is the hardness characteristics of Cu/Ni multilayers produced using electrodeposition. It comprises a relatively systematic study of the possible factors that can influence the hardness of a multilayered material. Chapter 2 provides theoretical background in electrochemistry, X-ray diffraction and hardness properties; chapter 3 details the experimental aspects in electrodeposition and hardness measurement; chapter 4 is a report of the experimental results and chapter 5 contains discussions.

Chapter 2

Theoretical background

2.1 Superlattice structure and growth of superlattices

2.1.1 Structural and chemical orders of superlattices

Superlattice is a type of artificially produced structure in which two different materials are alternatively layered upon each other in the nanometre-scale dimensions, as shown in Figure 1.1.

More information is needed to describe the structure of a superlattice than a homogeneous film. Superlattice can be categorized in terms of their structural and chemical order[15]. The structural order refers to the crystalline state, i. e., single crystal, polycrystalline, or amorphous, of the layers that make up the superlattice. The chemical order refers mainly to the period Λ and amplitude A of the composition modulation. Figure 2.1 shows two extreme cases of the composition modulation in an A/B superlattice: a square-wave modulation occurs when there is no mixing between the A and B layers and a low-amplitude sinusoidal modulation occurs when there is considerable intermixing between A and B.

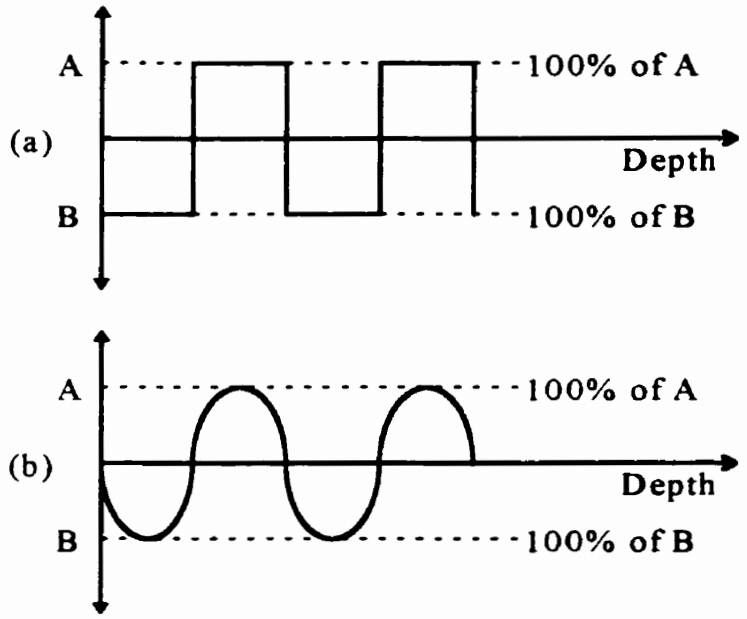

Figure 2.1: Schematic depiction of composition modulations in artificial superlattices showing (a) a square-wave modulation and (b) a small-amplitude sinusoidal modulation

The chemical order also refers to variations in layer thickness, i.e., variations in the Λ value, and interface roughness, i.e., deviations from a purely one-dimensional modulation as shown in Figure 2.2.

Figure 2.2: A schematic diagram showing the possible roughness of interfaces in a superlattice in contrast to the purely one-dimensional structure as shown in figure 1.1

In practice, all combinations of structural and chemical order may be observed in superlattices.

As the various properties of a superlattice are largely determined by its structural and chemical orders, it is necessary to understand how superlattices acquire their structural and chemical orders, i.e., the mechanisms of superlattice formation.

2.1.2 Mechanisms of superlattice growth

Three mechanisms governing the formation of thin films in general and of superlattices in particular have been proposed[18]: (a) the layer-by-layer growth (Frank-van der Merwe or FM mechanism); (b) a three-dimensional nucleation, forming, growth, and coalescence of islands (Volmer-Weber or VW mechanism); and (c) adsorption of a monolayer and subsequent nucleation on top of this layer (Stranski-Krastanov or SK mechanism). Which mechanism actually dominates in the formation of a superlattice depends on the strength of interaction between the atoms of the growing film and between the atoms of the film and the substrate.

Simple energetic arguments are often used to predict the growth mechanisms of a superlattice[15]. The FM nucleation takes place if the surface energy is reduced when covering an A surface with B. The surface energy is defined as the reversible work done on a system by the external forces to create a unit surface area at constant temperature. In terms of W_A and W_B, the vacuum surface energies of A and B, respectively, and W_{AB}, the energy of the A-B interface, FM nucleation of B on A results if

$$W_B + W_{AB} \leq W_A. \tag{2.1}$$

When A is subsequently deposited on B, the condition for FM nucleation is:

$$W_A + W_{AB} \leq W_B. \tag{2.2}$$

The most common case when both equation (2.1) and (2.2) are satisfied is when A and B have similar chemical and structural properties so that $W_{AB} \cong 0$ and $W_A \cong W_B$, as in Ag/Au superlattice. Another case in which both equations (2.1) and (2.2) can be satisfied is when A and B react strongly so that W_{AB} is negative.

There are many material combinations for which equations (2.1) and (2.2) are not satisfied simultaneously. If A has a much higher surface energy than B, that is $W_A >> W_B$, layer A will nucleate as three-dimensional (3-D) islands and the VW mechanism takes place. Another common case is when A and B are much different either chemically or structurally so that W_{AB} is large and positive. Depending on the values of W_A and W_B, one or both layers will nucleate through the VW mechanism.

The SK mechanism works when the structural and chemical differences between A and B are small. In this case, an intermediate nucleation mechanism is observed where 3-D islands form after one or more complete layers have been deposited.

The structural difference between two materials A and B can be represented by the lattice misfit (or mismatch) ε which is defined as:

$$\varepsilon = 2(d_A - d_B)/(d_A + d_B) \tag{2.3}$$

where d_A and d_B are the stress-free layer lattice spacings of materials A and B respectively. The superlattice mismatch ε plays an important role in determining the characteristics of the interfaces. Superlattices with larger ε have less planar interfaces than those with smaller ε[15].

In most cases, there is a considerable lattice misfit ε between the two materials A and B and therefore the VW mechanism takes effect. It has been found[18] that the growth of superlattice layers by the VW mechanism can be divided into the following three stages:

(a) Nucleation. Atoms of the depositing material reach the substrate and are attracted to the surface by forces mostly of dipole or quadruple character. They become, at least for a certain time, adsorbed on the surface and become adatoms. These adatoms are statistically distributed over the substrate and form nuclei for further growth;

(b) By surface diffusion. Some adatoms become attached to the surface of the already existing nuclei and form individual islands, which often have the shape of small crystals (crystallites);

(c) Coalescence of the islands and formation of a more or less connected network containing empty channels. Coalescence may happen three ways: (1) Ostwald ripening: a larger nucleus grows by engulfing a smaller one close to it. This process is slow and it happens mostly in treatment after deposition (Figure 2.3 (a)). (2) Coalescence due to mobility of islands: Smaller nuclei are more mobile than larger ones. They move and get absorbed by larger ones (Figure 2.3 (b)). This process is also too slow to play a significant role in deposition. (3) Coalescence by growth: this is the most important one. If two growing particles touch each other, they can - depending on the substrate temperature

and the surface energies - either agglomerate by retaining their shapes almost entirely or go through a liquid-like coalescence (at higher substrate temperatures or if the film is amorphous) process to form a single larger one (Figure 2.3 (c)).

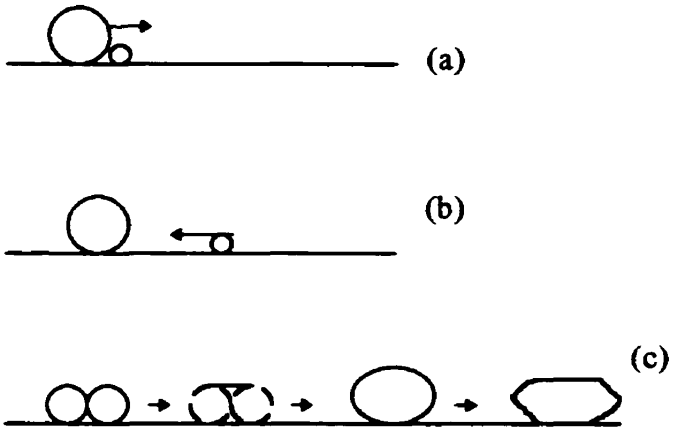

Figure 2.3: Three ways of coalescence: (a) Ostwald ripening; (b) cluster mobility; and (c) coalescence by growth

The three stages of superlattice growth are shown schematically in Figure 2.4.

Figure 2.4: Three stages in the formation of superlattice layers

2.1.3 Formation of the orientation of superlattices

Superlattices have a crystalline structure. The structure of a superlattice depends on its constituent materials, the deposition method, which determines the growth pattern of the thin film, the substrate on which it is deposited and some other factors.

Crystals growing on a substrate may be variously oriented. The possible orientations are shown in Figure 2.5. Case (a) illustrates a completely disordered film, in which the directions of axes of individual crystallites are distributed randomly. Case (b) describes a state in which one particular axis of all the crystallites is oriented in approximately the same direction. This is called a first-stage orientation or a single texture. Case (c) depicts the second-stage orientation or double texture. Finally, case (d) depicts a monocrystalline orientation, which is very important because it includes also the case of epitaxial films.

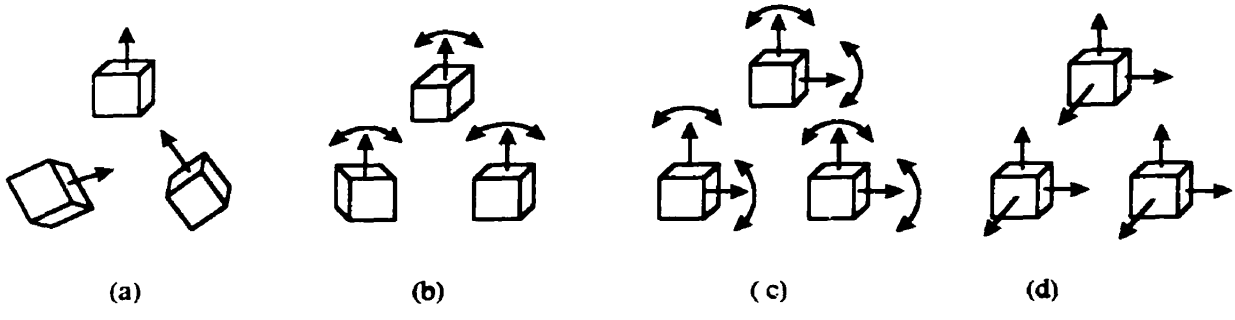

Figure 2.5: Orientation of crystallites on substrates. (a) chaotic ordering; (b) single fiber texture; (c) double texture; (d) monocrystalline orientation (double arrows indicates departures from prevailing orientation)

An important phenomenon in thin film growth is the epitaxial growth of a superlattice, that is, the formation of monocrystalline films on monocrystalline substrates either of the same substance or of another substance. The resulting orientation of the thin film depends on the crystal structure and orientation of the substrate. Epitaxy can occur

between materials of different crystal structure and of different chemical bonding. Observation of film structure during their preparation reveals that epitaxy begins to take place in the nucleation stage, but the stages of growth and coalescence of islands can be decisive for the final structure of the film.

The nuclei growing on a substrate may initially have various crystallographic orientations. It has been established though that when two islands which are of different sizes and crystallographic orientations coalesce, the resultant crystallite assumes as a rule the orientation of the larger one. This means that the growth conditions will determine the final orientation of a superlattice, that is to say, the superlattice will eventually adopt the orientation of the nuclei that the growth conditions are most in favor of.

In some cases when the substrate has a lattice constant approaching that of the film (the difference between them being less than 0.2%), "pseudomorphism" occurs and the film assumes the structure of the substrate until a thickness of the order of 10 nm is reached. If the difference is greater and the binding between the substrate and the film is strong, pseudomorphism occurs for only the earliest atomic layers. Still greater differences are accompanied by the formation of lattice defects (e.g., dislocations).

An important variable defining superlattice structure is the strain state of the layers. This is represented by the superlattice misfit:

$$\varepsilon = \varepsilon_{coh} + \varepsilon_{dis} \tag{2.4}$$

where ε_{coh} is the coherency strain and ε_{dis} is the portion of the mismatch accommodated by dislocations.

During the initial stages of depositing B on A, B is strained such that its lattice parameter matches that of A, i.e., the A/B interface is coherent and ε_{coh} is at its maximum. Upon further deposition, the interfacial coherency is lost by the introduction of interfacial misfit dislocations, which either partially or fully relax the lattice spacing of B to its stress-free value. When B is completely relaxed, $\varepsilon_{coh} = 0$.

An estimate of the coherency strain ε_{coh} expected in a layer is given by [15]:

$$\varepsilon_{coh} = \left(\frac{D}{2Bh}\right) \ln\left[\left(\frac{h}{b}\right) + 1\right] \tag{2.5}$$

In equation (2.5),

$$B = \frac{2G_f(1+\nu)}{(1-\nu)} \tag{2.6}$$

where G_f is the shear modulus of the film material, ν is the Poisson's ratio which is related to the shear modulus G and elastic modulus Y by $Y = 2G(1+\nu)$, and

$$D = \frac{G_f G_s b}{\pi(G_f + G_s)(1-\nu)} \tag{2.7}$$

where G_s is shear modulus of the substrate. In deriving equation (2.5), it is assumed that the film thickness $h < 2s$, where $s = b/(\varepsilon - \varepsilon_{coh})$ is the separation between dislocations and b is the Burger's vector.

For small enough film thickness h, equation (2.5) gives $\varepsilon_{coh} > \varepsilon$. This is physically unacceptable, but rather implies that the film is strained to match the underlying material without misfit dislocations. As h increases, ε_{coh} will decrease until $\varepsilon_{coh} < \varepsilon$. A fraction $(\varepsilon - \varepsilon_{coh})/\varepsilon$ of the mismatch will then be accommodated by dislocations. Since ε_{coh} continues to decrease as h increases, the film approaches complete relaxation with continued deposition. A critical thickness h_c can be determined[15] using the condition $\varepsilon = \varepsilon_{coh}$:

$$h_c = \left(\frac{D}{2B\varepsilon}\right)\left[\ln\left(\frac{h_c}{b}\right) + 1\right] \tag{2.8}$$

for single layer film, and

$$h_c = \frac{b(1 - \nu\cos^2\psi)[\ln(\frac{h_c}{b}) + 1]}{2\pi\varepsilon(1+\nu)\cos\phi} \tag{2.9}$$

for multilayer films. Where, ψ is the angle between dislocation line and its Burgers vector and ϕ is the angle between the slip direction and the direction in the film plane that is perpendicular to the interface/slip plane intersection.

At thickness h_c, it is energetically favorable for misfit dislocations to form. The dependence of h_c on ε is shown in Figure (2.6) [15].

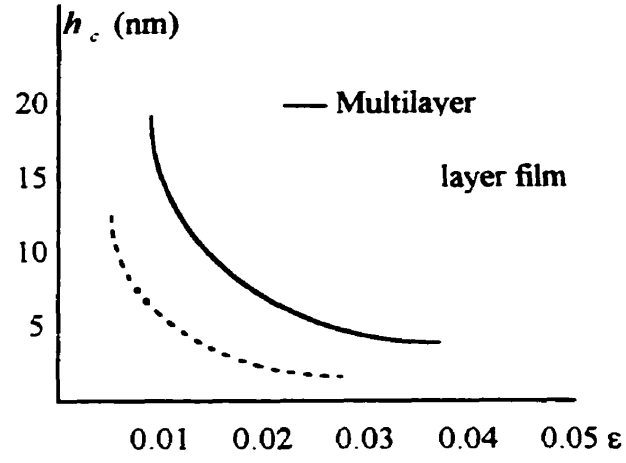

Figure 2.6: Dependence of critical thickness h_c on superlattice misfit ε

The critical thickness for multilayered films is larger than that for single layer film. This is because the strain is divided between the depositing layer and the underlying layers.

2.1.4 Crystallographic structure of copper and nickel

For the copper and nickel system studied in this work, both constituent materials have the fcc structure as shown in figure 2.7.

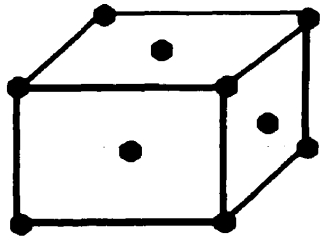

Figure 2.7: The fcc structure of Cu and Ni crystals

Their lattice constants d are 3.615 and 3.526 angstroms respectively with an interface misfit ε of 2.5% for the {100} Cu and {100} Ni interplanar spacings. The

mismatch value indicates that a VM mechanism will take place in the growth of the Cu/Ni superlattice, and on a copper substrate with prevailing (100) orientation, the superlattice will have a dominant (100) orientation. This is confirmed in the experimental part.

2.2 Electrochemistry

2.2.1 Fundamental equation for an electrochemical cell

Electrodeposition refers to the process of depositing a material (typically metal) from a solution (called electrolyte) on another one through an electrochemical reaction. It was first used to make multilayers in 1921, when Blum[19] deposited copper/nickel and other multilayered films by alternate deposition from two different electrolytes. This is called dual-bath deposition. Later, multilayers have been produced from a single electrolyte which contained two or more kinds of metal ions. This is called single-bath deposition. By getting rid of the trouble of mechanically switching the samples between two baths, the single-bath method is simpler to implement and it allows multilayers with graded interfaces to be made by tailoring the deposition waveform. However, it is restricted to certain pairs of materials or composition ranges because of the requirement for a compatible electrolyte and the limited range of alloy compositions that can be deposited from a given electrolyte. Also, it is impossible to deposit a pure layer of the less noble metal (a less noble metal requires a more negative reduction potential) with a single-bath. The most successful single-bath multilayer deposition technique is the one developed by Tench & White[20] and Yahalom & Zadak[21]. The single-bath technique is preferred by most researchers and is the choice in this work. By controlling the compositions of the

two materials in the electrolyte and the proper selection of deposition parameters, even the less noble material can achieve very high purity in the multilayers.

An electrochemical reaction (or electrode reaction) involves not only molecules and ions, but also negative electrons e^- arising from a metal or other substance by metallic conduction. Such a reaction is called oxidation if it proceeds in the direction corresponding to the liberation of electrons; and it is called a reduction if it proceeds in the direction corresponding to the absorption of electrons. For example,

Oxidation: $Cu \rightarrow Cu^{2-} + 2e^-$

Reduction: $Ni^{2-} + 2e^- \rightarrow Ni$

To understand how an electrochemical reaction occurs, it is helpful to start with the electrode reactions (electrode processes).

If a metal electrode is immersed in a solvent (water in this work), some of the metal ions will be freed from the binding of their metal lattices due to collisions from the molecules of the solution and enter the solution. As the concentration of the metal ion in the solution increases, some ions will be re-absorbed and neutralized by the electrode surface and eventually an equilibrium state will be reached between these two processes. At this stage, the number of ions entering the solution equals the number of ions reabsorbed and neutralized at the electrode. After the ions leave the surface of the electrode, a layer of electrons will be accumulated at the electrode surface. These electrons then attract a layer of ions to them, forming an electrical double layer as shown in Figure 2.8.

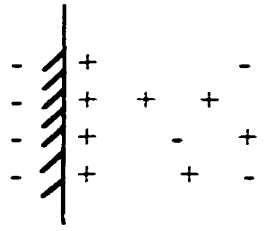

Figure 2.8: Schematic diagram of electrical double layer

As a result, a potential difference is established between the electrode and the solution. In practice, this potential is characterized by the standard electrode potential U^0.

The standard electrode potential is defined as the potential of a cell in which the hydrogen electrode is on the left and all components of the cell are at unit activity. The activity a_i for reactant i in a solution is defined by

$$a_i = \frac{\gamma_i m_i}{m^0} \tag{2.10}$$

where, m_i is the molality, which equals to the amount of electrolyte per kilogram of solvent, which is given by $n_i/M_1 n_1$, where n_i is the amount of electrolyte in n_1 mole of solvent and M_1 is the molar mass of the solvent; m^0 is the standard value of the molality (1 mol/kg of solvent); and the activity coefficient γ_i is defined by:

$$\lim_{m_i \to 0} \gamma_i = 1 \qquad (2.11)$$

This potential is attributed entirely to the electrode reaction in the right-hand electrode; that is, the standard electrode potential of the standard hydrogen electrode H^+ (a=1) | H_2 (1 bar) | Pt is arbitrarily assigned the value zero so that its electrode reaction and standard electrode potential are given by:

$$H^+ + e^- = \frac{1}{2} H_2 (g) \qquad U^0 = 0.0000V \qquad (2.12)$$

Electrochemical reactions (or electrode processes) differ from chemical reactions in that they involve not only chemical reagents but also an electric reagent (the negative electron) which acts at the interface between a metal and a solution of electrolytes. The difference between the actual electrode potential E_a of the metallic surface and the equilibrium potential E of the reaction is called the overpotential η:

$$\eta = E_a - E \qquad (2.13)$$

If η = 0, the thermodynamic equilibrium of the reaction is obtained; if η > 0, the reaction takes place in oxidation direction; if η < 0, the reaction takes place in reduction direction.

If two electrodes are immersed in a bath containing an electrolyte, an electrochemical reaction will take place and the bath is called an electrochemical cell.

Electrochemical cells can be classified as galvanic cell and electrolytic cell as shown in Figure 2.9:

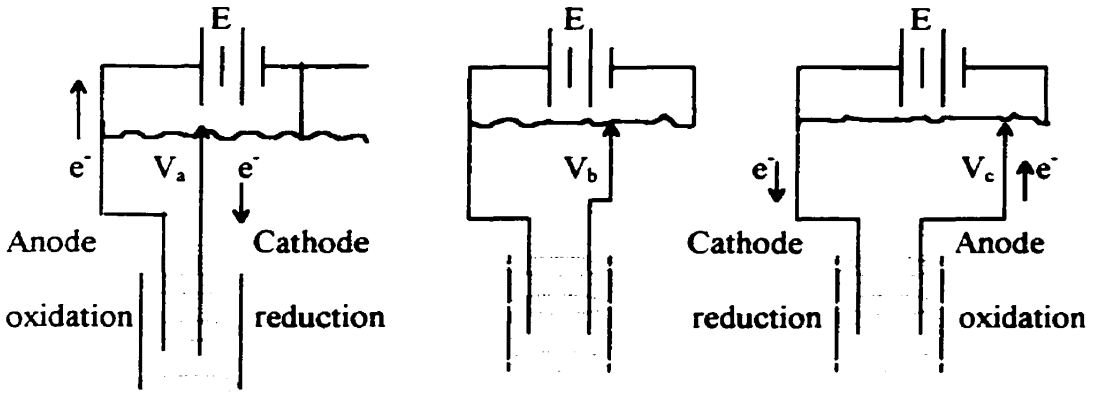

(a) Galvanic cell (b) Cell at equilibrium (c) Electrolytic cell

Figure 2.9: Electrochemical cells for three different kinds of reactions: (a) reduction on the right ($V_a < E$); (b) no reaction ($V_b = E$); and (c) oxidation on the right ($V_c > E$)

In a galvanic cell, chemical reaction occurs spontaneously while in an electrolytic cell chemical reaction is caused by an externally applied potential. The electrode where a reduction reaction occurs is called the cathode and the electrode where oxidation occurs is called an anode.

In Figure 2.9 (b), V_b, the electric potential applied to the two electrodes, is equal to E, the equilibrium potential difference of the cell, so no current passes the cell. This potential is called the electromotive force (emf) of the cell. If the applied potential difference is less than the electromotive force, the cell discharges spontaneously and it is called a galvanic cell as shown in Figure 2.9 (a); when the applied potential is increased to a value beyond the electromotive force as shown in Figure 2.9 (c), it drives the cell reaction in the reverse direction and the cell is referred to as an electrolytic cell.

The electromotive force E can be expressed in terms of the activities of the reactants and products[22]:

$$E = E^0 - \frac{RT}{nF} \ln \prod_i a_i^{\upsilon_i} \tag{2.14}$$

Equation (2.14) is called the Nernst equation in which E^0 is the standard electromotive force of the cell, the electromotive force when the activities of all reactants and products are equal to unity; R is the gas constant; T is thermodynamic (absolute) temperature; n is the charge number of an electrochemical reaction (the number of electrons transferred per reaction); F is the Faraday constant; a_i is the activity of reactant i and υ_i is the stoichiometric number for reactant i. The stoichiometric number υ_i is the number of molecules participated in the reaction. It is positive for products and negative for reactants.

The importance of equation (2.14) lies in the fact that it reveals the dependence of the electromotive force on electrochemical reaction and the electrolyte in an electrochemical cell. Different electrolytes and different reactions have different electromotive forces. Therefore, in a solution which contains two or more types of metal ions, different reactions may be activated by changing the applied potentials. This is the underlying mechanism with which a single-bath works in the deposition of multilayer thin films.

Several empirical methods have been established to determine the value of E^0 and γ_i for a variety of electrolytes[22][23]. The electromotive force E for a certain electrolyte can then be calculated using equation (2.14).

One of the useful tools in calculating the standard potential E^0 of a cell is the standard electrode potentials table[22][24], in which the standard electrode potentials of a variety of electrodes are listed. For any cell with two electrodes, the standard electromotive force of the cell E^0 can be calculated using

$$E^0 = U_R^0 - U_L^0 \tag{2.15}$$

where U_R^0 and U_L^0 are the standard electrode potentials of the right and left electrodes respectively.

2.2.2 The electrochemical reactions in the Cu/Ni multilayer bath

From the standard electrode potentials table[22], we know that for the reaction

$$Cu^{2+} + 2e^- = Cu \tag{2.16}$$

the standard electrode potential is 0.3394V; and for the reaction

$$Ni^{2+} + 2e^- = Ni \tag{2.17}$$

the standard electrode potential is -0.25V.

It should be noted that these potentials are the standard electrode potentials as defined above and are not the real potentials that should be used in the real experiments. However, they indicate that copper has a higher reduction potential (or less negative potential) than nickel, therefore we say copper is a more noble metal and nickel is a less noble metal. The real reduction potentials for each of the two metals in a certain electrolyte can be experimentally determined using a voltammogram. A voltammogram is a diagram which shows the current dependence on the potential applied to an electrochemical cell as is shown in Figure 2.10.

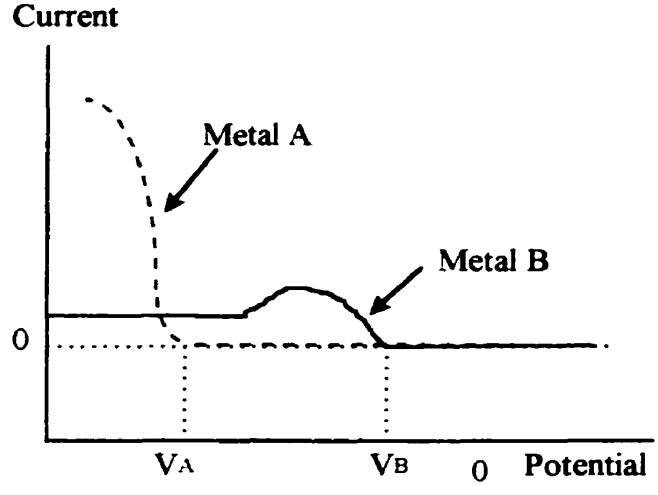

Figure 2.10: Schematic diagram showing the current dependence on potential for an electrolyte containing metal A and B with metal A having a much higher concentration than metal B.

Starting at potential V_B, reduction of metal B begins and a current can be detected at the cathode. From V_B down to the potential at V_A, only metal B is reduced. As the potential further decreases from V_A, both metal B and metal A are reduced. The current increases sharply because metal B has a much higher concentration in the electrolyte.

Theoretically, any potential value in the range of between V_B and V_A can be used to reduce metal B only; and any value lower than V_A can be used to deposit metal A with a certain impurity of metal B. To alternatively deposit metal A and B, a potential waveform as shown in Figure 2.11 can be applied:

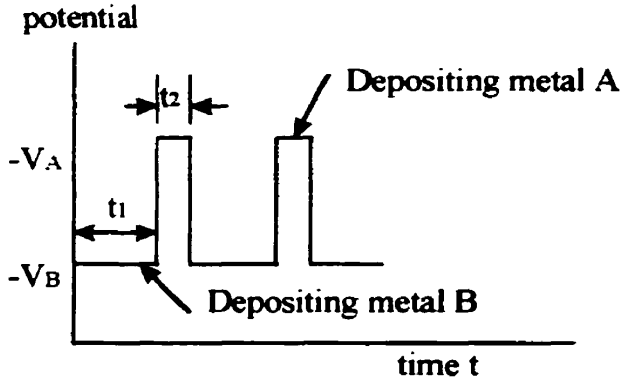

Figure 2.11: Potential waveform for the alternating deposition of metal A and B (not in scale)

As is shown in Figure 2.10, at less negative over-potentials, only the more noble metal B can be reduced and as a result a pure layer of metal B can be obtained during the deposition period t_1 shown in Figure 2.11. At more negative over-potential during deposition period t_2, both metal A and B are reduced and as a result an alloy of the two metal is obtained. This is one of the major drawbacks in the deposition of multilayers using a single-bath. It's impossible to obtain a pure layer of the less noble metal. However, if the ratio between the concentrations of metal B and A in the electrolyte is made large enough, the purity of metal B in the alloy layer can be made as high as desired. There is, of course, a trade-off in the requirement for deposition time. Lower concentration in metal B requires longer deposition time to obtain a certain thickness of metal B. The time needed to deposit a certain thickness of a metal can be calculated using Faraday's Law.

Faraday's law states that "in electrolysis, 96,500 Coulombs of electric charge produce chemical charge of 1 g equivalent." Let's consider a reduction reaction of metal M:

$$M^{n-} + n(e^-) \rightarrow M. \tag{2.18}$$

If the desired thickness is d (in cm) and the sample has a circular shape with a radius r (in cm), the mass m (g) of the metal required to be deposited from the electrolyte is given by:

$$m = \pi r^2 d\rho \tag{2.19}$$

where ρ is the density of material M in the unit of g/cm^3. The gram equivalent m_g of this mass is:

$$m_g = m / m_a = \pi r^2 d\rho / m_a \tag{2.20}$$

where m_a is the atomic mass of material M.

From reaction (2.18), we know that to produce 1 gram equivalent of material M, we need n gram equivalent of electrons. The total electrons m_{eg} (in gram equivalent) needed to produce m_g gram equivalent of material M is therefore:

$$m_{eg} = nm_g = n\pi r^2 d\rho / m_a \tag{2.21}$$

From Faraday's Law, the total charges Q (in Coulomb) needed to produce m_{eg} gram equivalent of electrons is:

$$Q = Fn\pi r^2 d\rho / m_a \tag{2.22}$$

where F = 96.500 is Faraday's constant.

Suppose the current during the deposition of metal M is I and is kept constant (this is a reasonable assumption for most experiments), the charges passed during time t (in second) is:

$$Q = It \tag{2.23}$$

Combining equation (2.23) with equation (2.22) gives:

$$t = nF\pi r^2 d\rho / m_a I \tag{2.24}$$

This is the time required to deposit metal M with a thickness of d and a radius of r. It is in inverse proportion to current I. As I is in direct proportion with the concentration of metal M in the electrolyte, I is therefore in inverse proportion to the concentration. In a typical Cu/Ni multilayer deposition bath, the ratio of concentrations between Cu and Ni is about 1:100 and accordingly the deposition currents for the two metals also have a ratio of around 1:100. Therefore, to deposit the same thickness of the two metals, the time needed for Cu is about 100 times that for Ni.

The purity of the Ni layer can be estimated using equation (2.24). The mass deposited during time t is obtained by rewriting equation (2.24):

$$m = \pi r^2 d\rho = t m_a I / nF \tag{2.25}$$

For the Cu and Ni reductions represented by equation (2.16) and (2.17), the masses for Ni and Cu deposited during time t are given respectively by equation (2.26) and (2.27):

$$m_{Ni} = t m_{aNi} I_{Ni} / 2F \tag{2.26}$$

$$m_{Cu} = t m_{aCu} I_{Cu} / 2F \tag{2.27}$$

Therefore the purity of Ni is expressed as:

$$p_{Ni} = \frac{m_{Ni}}{m_{Ni} + m_{Cu}} = \frac{m_{aNi} I_{Ni}}{m_{aNi} I_{Ni} + m_{aCu} I_{Cu}} \tag{2.28}$$

For a bath with a current ratio of 1:100 between Cu and Ni, equation (2.28) gives a purity estimate of 98.9% for the nickel layer. In most experiments, the current ratio is even smaller and therefore the purity of the Ni layer is even higher than this estimate.

2.3 X-Ray crystallography

As a non-destructive testing technique, x-ray diffraction is a powerful tool for the analysis of crystalline structure. X-ray has wavelengths[25] comparable to the crystalline lattice constants, thus it can be used for the accurate measurement of crystalline parameters.

Theories have been developed for x-ray diffraction in superlattices. Interpretation of x-ray diffraction patterns from superlattices provides most of the important information about the structural characteristics of superlattices.

2.3.1 Crystalline structure

An ideal crystal can be viewed as a spatial repetition of a basic cell which is defined by three fundamental vectors $\bar{a}, \bar{b}, \bar{c}$ as is shown in Figure 2.12.

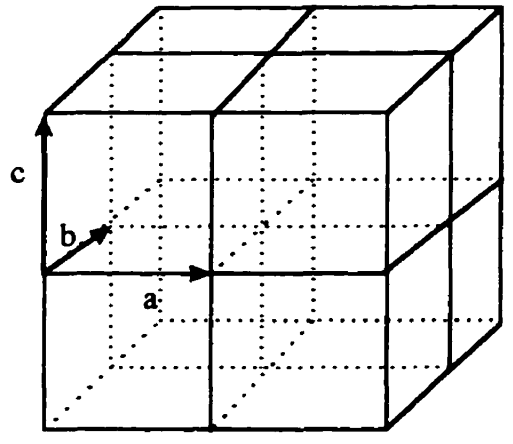

Figure 2.12: An ideal crystal structure and the three fundamental vectors

The repetition of the basic cell constructs a lattice in space. A base, sometime one, atom is attached to each of the lattice point. The atoms form groups of parallel planes which define the various orientations of the crystal. The direction of a group of parallel planes can be denoted by the Miller index which is defined as follows:

Suppose a plane intercepts the three axes $\vec{a},\vec{b},\vec{c}$ at positions $P_1\vec{a},P_2\vec{b},P_3\vec{c}$ where P_1,P_2,P_3 are integers (not all zeros). The miller index for the set of planes parallel to the one selected is given by the following formula:

$$(hkl)=(\frac{1}{P_1},\frac{1}{P_2},\frac{1}{P_3})P_{1,2,3} \tag{2.29}$$

where $P_{1,2,3}$ is the smallest common multiple of P_1, P_2, P_3. If any one of the integers P_1, P_2, P_3 is zero, that is, the plane is parallel to some axis, the corresponding Miller index number is represented by 0. Figure 2.13 shows several important planes with their Miller indices.

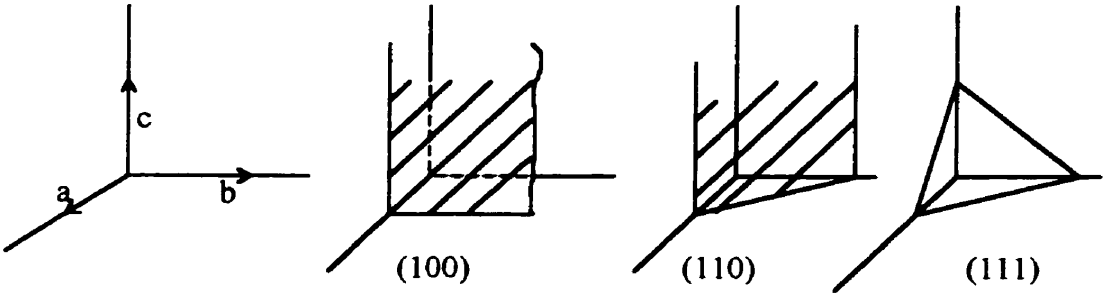

Figure 2.13: Several important planes and their Miller indices

The perpendicular distance between two adjacent parallel planes is a parameter characterizing the structure of a crystal. For the group of planes with Miller index (hkl) in a cubic lattice, it is given by[26]:

$$d_{hkl} = \frac{a}{\sqrt{h^2 + k^2 + l^2}} \tag{2.30}$$

2.3.2 Bragg's law

If an x-ray beam is incident on a crystal surface, the x-ray beam will be scattered by the atoms on the crystalline lattice as is shown in Figure 2.14.

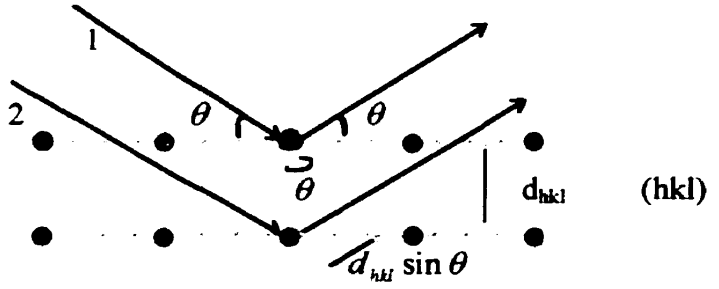

Figure 2.14: Scattering of X-ray by atoms on a crystal lattice

If the inter-planar spacing d_{hkl} and the incident angle θ satisfy the following equation:

$$2d_{hkl} \sin\theta = n\lambda \tag{2.31}$$

where λ is the wavelength of the X-ray beam and n is an integer, the scattered beam will be reinforced and a maximum of diffraction will be detected. Equation (2.31) is called Bragg's law. It can be explained as follows:

The difference in the distances traveled by ray 1 and ray 2 is $2d_{hkl}\sin\theta$ as indicated in Figure 2.14. If this difference is an integral multiple of the X-ray wavelength, the two rays will interfere constructively.

The Bragg's law requires that λ and θ be matched by equation (2.31): x-rays of wavelength λ incident on a crystal at arbitrary angle will in general not be reflected. To satisfy the Bragg's law, it is necessary to scan a wide range of either the angle or the wavelength. Experimentally, it is usually the angle that is scanned while the wavelength is kept fixed. As a result, different groups of atomic planes with different Miller indices will be brought into position for reflection and a diffraction spectrum like the one shown in Figure 2.15 will be obtained.

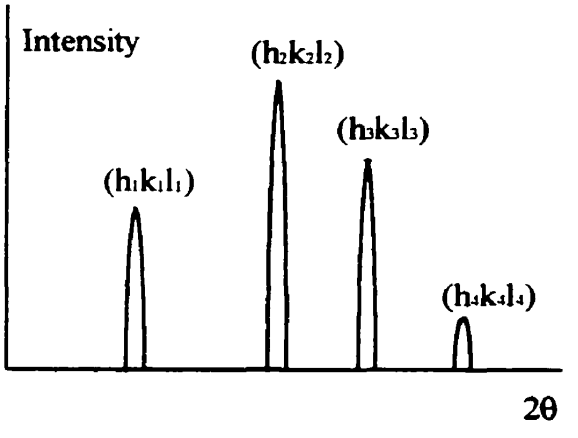

Figure 2.15: A schematic x-ray diffraction diagram; θ is the incident angle.

Some data of x-ray diffraction for copper and nickel[27] are presented in table 2.1.

Table 2.1 X-ray diffraction constants for Cu and Ni

Radiation: Cu, $K_{\alpha 1}$, $\lambda = 1.5405\ \mathring{A}$

(hkl)		(111)	(200)	(220)	(311)	(222)
d_{hkl} (A)	Cu	2.088	1.808	1.278	1.090	1.0436
	Ni	2.034	1.762	1.246	1.0624	1.0172
θ	Cu	43.298	50.434	74.132	89.934	95.142
	Ni	44.507	51.847	76.372	92.948	98.448

2.3.3 X-Ray diffraction in superlattices

Superlattices differ structurally from their bulk materials in that in one direction the periodicity is interrupted by the interfaces between the two different layers. The X-ray diffraction patterns of superlattices are therefore also different from that of the bulk materials. The most prominent phenomenon in the X-ray diffraction diagrams from superlattices is the appearance of second or even higher order reflection peaks (called satellites) that surround the main Bragg peak. A typical X-ray diffraction diagram from a superlattice resembles the one shown in Figure 2.16.

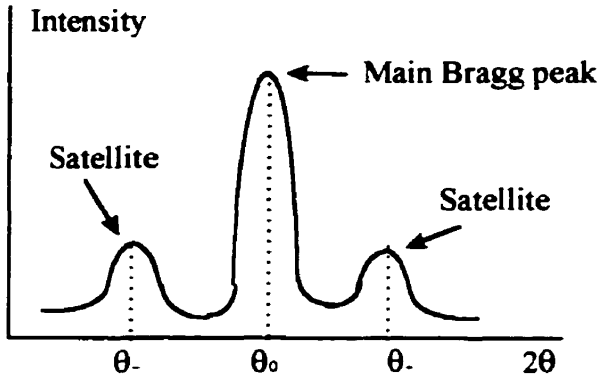

Figure 2.16: Schematic diagram showing satellites from x-ray diffraction from superlattice

If the lattice mismatch between the two constituent materials in their relaxed states is small as in the case of copper and nickel, the two Bragg peaks from the constituent materials will overlap and result in a broadened main Bragg peak with its center lying in between the two Bragg angles of the constituent materials. Interference between the two materials will in addition produce satellites which shoulder the main Bragg peak.

Application of scattering theory[28] to superlattice structure relates the positions of the two first-order satellites to the superlattice periodicity through equation (2.32):

$$\Lambda = \frac{\lambda}{\sin\frac{\theta_+}{2} - \sin\frac{\theta_-}{2}} \qquad (2.32)$$

Equation (2.32) can be used to experimentally determine the superlattice periodicity. It is also helpful in interpreting the appearance of an x-ray diffraction diagram. For instance, for small Λ, the separation between the two satellites is large and a diagram resembling figure 2.16 can be expected with sharp resolution of the two satellites; as Λ

increases, the separation between the two satellites narrows and at a certain value of Λ they can be so closely spaced that they will actually merge with the main Bragg peak, forming a big "envelop" as shown in figure 2.17. Therefore, a sample with large Λ producing an x-ray diffraction diagram such as the one in figure 2.17 may still be a well-layered superlattice.

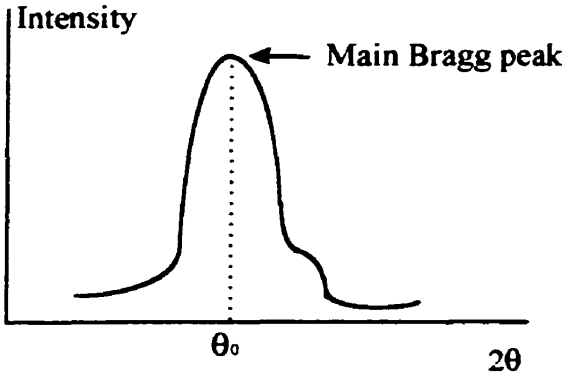

Figure 2.17: At large Λ, the satellites merge with the main Bragg peak and become irresolvable.

2.4 Hardness characteristics of superlattices

Hardness is a measure of a material's resistance to plastic deformation caused by surface indentation or abrasion. It is usually measured by pressing a diamond tip of a specially-designed shape into the surface of a sample. The hardness is then characterized by the size of the indentation. It is defined to be the force F divided by the indent area S, that is, H = F/S. Hardness is typically expressed in unit of Gigapascals (1 GPa = 10^6 N/m^2). There are a number of ways in hardness measurement, each of them using a different indentation tip and a different range of force applied. The interpretation of the

indentation area is key to determining the precision of the hardness measurement. These topics will be discussed in the section "Hardness measurement" in chapter 3.

When a material is subject to an external force, its mechanical structure will undergo a series of changes depending on the magnitude of the force applied. This process can be illustrated by the stress-strain curve as shown in Figure 2.18.

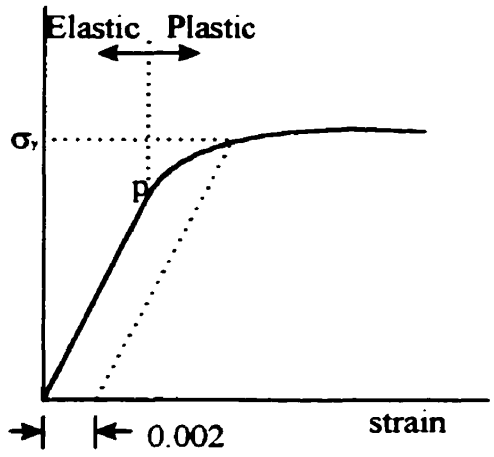

Figure 2.18: Stress-strain curve of a material

In Figure 2.18, the region from the origin to point p is the elastic deformation area in which the strain and stress are proportional and the deformation will vanish once the applied force is removed. The strain $\in$ and stress σ are related to each other according to Hooke's Law:

$$\sigma = Y \in \tag{2.32}$$

where Y is the elastic constant of the material.

Passing point p, the strain is no longer in proportion with the stress and the deformation becomes non-recoverable and permanent. This is the plastic deformation area. For most metallic materials, plastic deformation occurs at strain values around 0.005. In materials engineering, it is important to know at which stress level plastic deformation begins, that is the stress level at which the phenomenon of yielding occurs. Theoretically, this is the point at which the strain-stress curve begins to lose its linearity, as indicated by the point p in Figure 2.18. However, the transition from linearity to non-linearity is gradual and it is difficult to determine the point precisely. As a consequence, a convention has been established to find the yield strength of a particular material: a straight line is to be constructed parallel to the elastic portion of the strain-stress curve at some specified strain offset, typically 0.002. The stress corresponding to the point at which this line intersects with the strain-stress curve is defined as the yield stress σ_y, as indicated in Figure 2.18.

The yield strength of a material is a direct indication of its hardness. For crystalline materials, including superlattices, their hardness has been empirically established to be as about three times the yield strength[29]:

$$H = 3\sigma_y \tag{2.33}$$

As is pointed out earlier, hardness and yield strength are an indication of how easily a material deform plastically under the influence of an external force. From the atomic perspective, plastic deformation is a result of the breaking and reforming of atomic

bonds. This is accomplished by the generation and motion of microscopic line defects called "dislocations." When a force is applied onto the surface of a material, dislocations are generated and, together with the ones already in existence, they move in the material, causing crystal-lattice planes to slide across each other, a process called slip. This results in the permanent plastic deformation of the indented area. Hardness is therefore a measure of how readily dislocations are generated and are able to move in a material under an applied force.

A dislocation is a linear or one-dimensional structural defect in a crystalline material. Atoms around a dislocation are displaced from their normal lattice points. Figure 2.19 shows two fundamental types of dislocation common in crystalline materials:

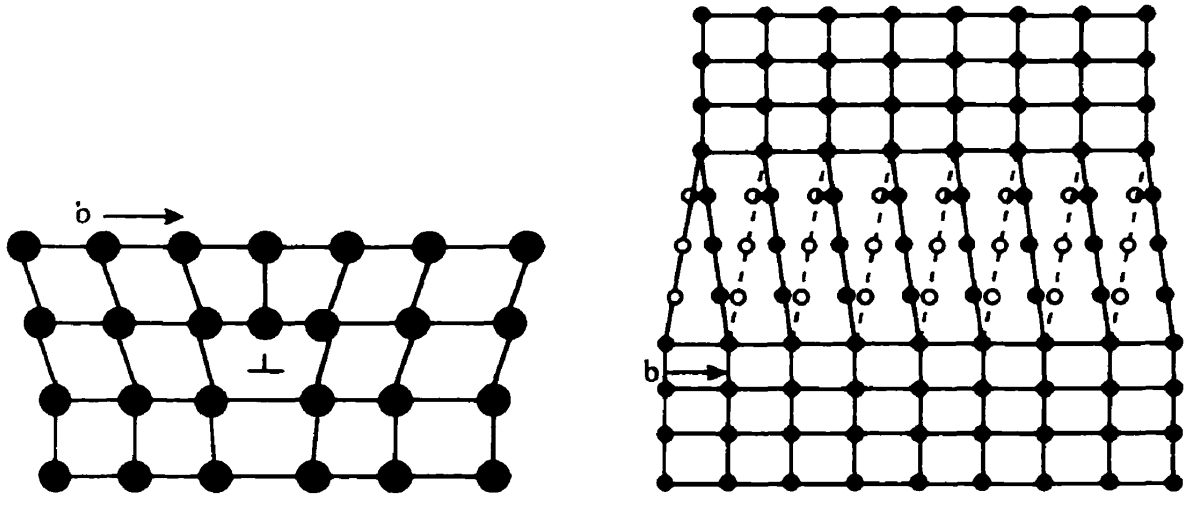

Figure 2.19: Schematic structure of dislocations: (a) edge type; (b) screw type

In the diagram, $\vec{b}$ is the Burgers vector which is an indication of the magnitude and direction of the lattice distortion around a dislocation. It is usually of the order of the

lattice spacing. For edge dislocations, if the extra half-plane of atoms is on the upper half of the crystal, it is represented by the sign "⊥"; if it is on the bottom portion of the crystal, it is represented by the sign "⊤".

Dislocations play an important role in regulating many of the mechanical properties of a material due to the strain fields that are entailed in the vicinity of dislocations. When a material deforms, some of the work done by the applied force during the deformation process is transformed into strain energy – the potential energy of the atoms which are displaced from their equilibrium positions. As a result, strain energy fields or, to put it simple, strain fields are generated around the dislocations. Strain fields can be divided into three types: compressive, tensile and shear. As is shown in Figure 2.19 (a), the atoms above the dislocation line are squeezed together while the ones below are pulled apart. Therefore, the strain field above the dislocation line is compressive-type and the one below tensile-type. The strain field around a screw dislocation is of shear-type.

The magnitude of the energy of the strain field around a dislocation is proportional to the elastic constant of the material and the degree of the distortion of the lattice structure as is reflected in the simple harmonic type potential energy:

$$E_p = \frac{1}{2} k\alpha^2 \tag{2.34}$$

The existence of strain fields is an important factor in the strengthening mechanism of crystalline materials as they affect the motion of dislocations due to their mutual

interactions. Dislocations of the same sign repel each other while the ones with different signs attract each other as is illustrated in Figure 2.20.

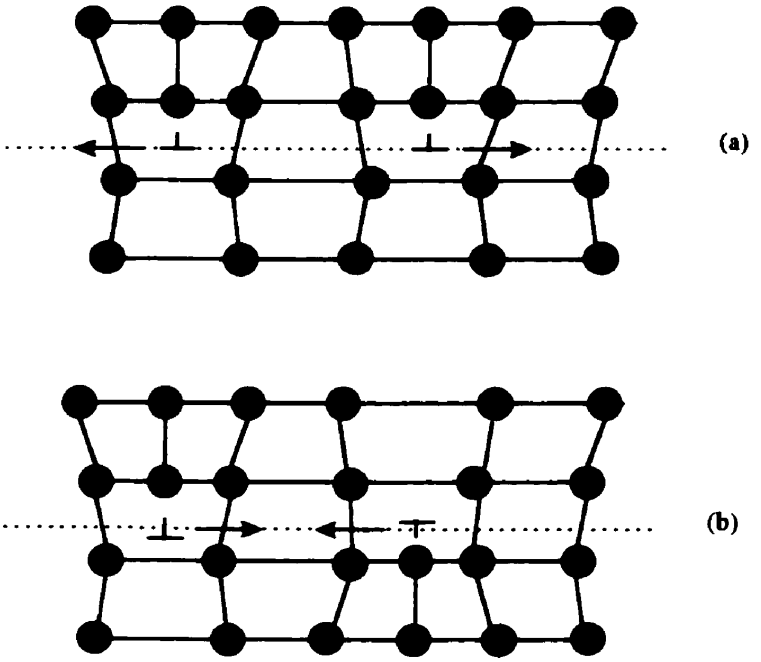

Figure 2.20: Interactions between dislocations: (a) same-sign dislocations repel each other; (b) opposite-sign dislocations attract each other

Plastic deformation occurs when a dislocation moves under the influence of an external force. Figure 2.21 shows how an edge dislocation moves in response to a shear stress applied in a direction perpendicular to the dislocation line which is perpendicular to the paper:

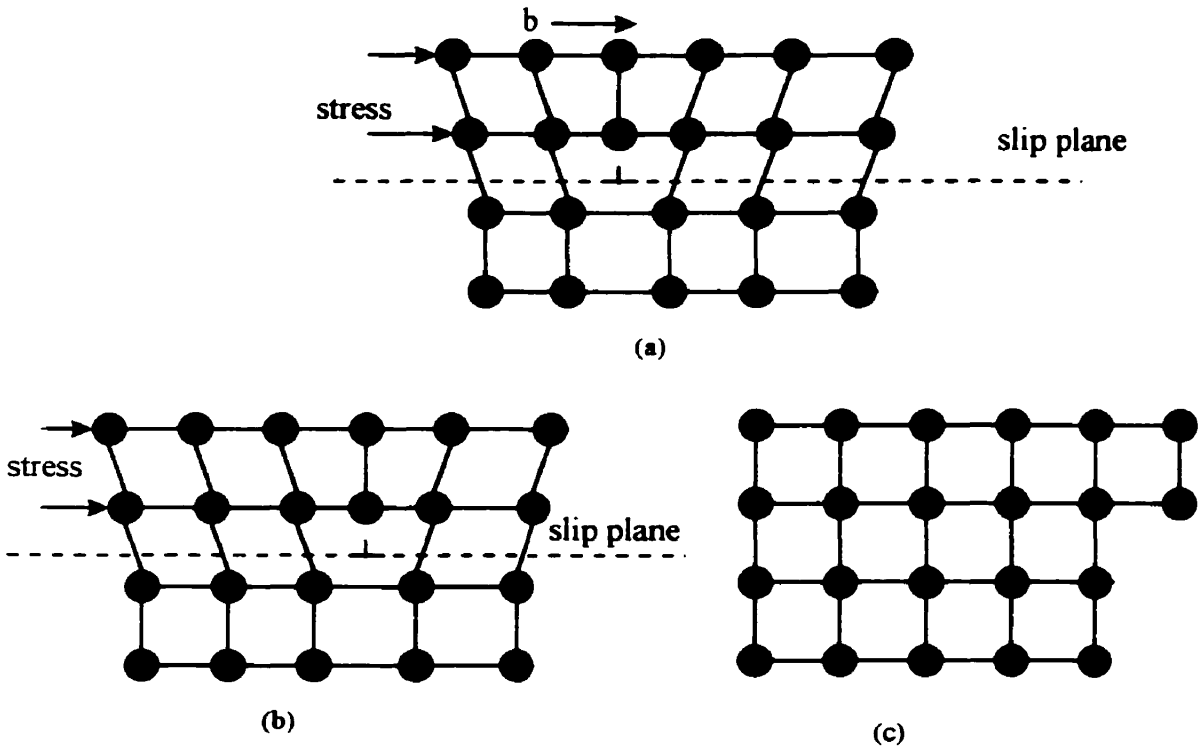

Figure 1.21: Motion of a dislocation: under a shear stress applied on the left of the crystal, the dislocation in (a) moves to the right in (b) and eventually bows out in (c)

For a certain crystal, there are specific crystallographic planes and specific directions on these planes along which dislocations move with the maximum degree of ease. These planes are called slip planes and the directions slip directions. The slip planes are the ones that have the most dense atomic packing and so do the slip directions. A slip plane and a slip direction constitutes a slip system. A slip system is characterized by the minimum lattice distortion when a dislocation moves along it. For fcc crystals like copper and nickel, the slip systems are formed by the {1,1,1} planes and the <110> directions. As a result, there are a total of 12 slip systems in a fcc crystal. The more slip systems a crystal has, the easier it deforms plastically because of the more possible choices in the paths along which the dislocations can move.

There exists a minimum shear stress to initiate the motion of a dislocation along a slip system in a crystalline material. This stress is termed the critical resolved shear stress σ_c and it can be used to determine the yield stress $\bar{\sigma}_y$ and subsequently the hardness of a material.

Suppose an external stress $\bar{\sigma}$ is applied to the surface of a material. The stress is oriented in a way such that it forms an angle of α with the normal of the slip plane of an arbitrarily-chosen slip system and an angle of β with its slip direction as shown in Figure 2.22:

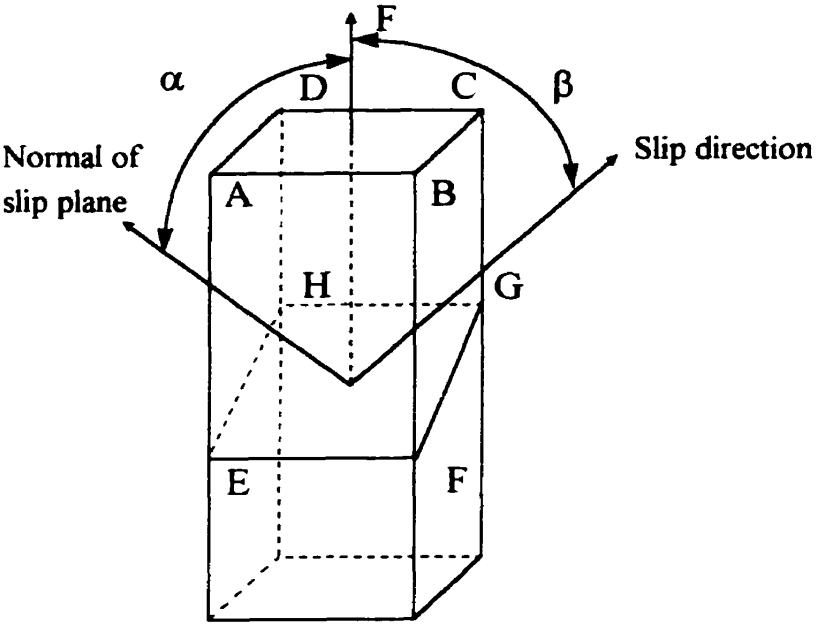

Figure 2.22: Orientation relationships among the applied tensile stress, slip plane and slip direction

In Figure 2.22, F is the applied force; ABCD is the surface plane and EFGH is a slip plane. The component of the applied force along the slip direction is:

$$F_s = F\cos\beta \tag{2.35}$$

The area of the slip plane is:

$$S_s = \frac{S}{\cos\alpha} \tag{2.36}$$

where S_s and S are the areas of plane EFGH and ABCD, respectively.

The stress on the slip plane along the slip direction is therefore given by:

$$\sigma_s = \frac{F_s}{S_s} = \frac{F}{S}\cos\alpha\cos\beta = \sigma\cos\alpha\cos\beta \tag{2.37}$$

σ_s is called the resolved shear stress. It is the component of the external stress that will drive the dislocation to move along this specific slip system.

As we already know, there are a number of slip systems in a crystalline material. These slip systems have different orientations with respect to the applied stress σ. There will always be a slip system which has the maximum value of the resolved shear stress $\sigma_{s\max}$:

$$\sigma_{s\max} = \sigma(\cos\alpha\cos\beta)_{\max} \tag{2.38}$$

This slip system is the most favorably oriented one which will initiate the motion of the dislocations. Let this stress be equal to the critical resolved shear stress σ_c, we obtain the stress required to apply to initiate the motion of dislocations:

$$\sigma_y = \frac{\sigma_c}{(\cos\alpha\cos\beta)_{max}} \tag{2.39}$$

this is the yield stress at which the material begins to deform plastically.

The hardness can be found using equation (2.33):

$$H = \frac{3\sigma_c}{(\cos\alpha\cos\beta)_{max}} \tag{2.40}$$

The above conclusion is drawn for single crystals. In the case of polycrystalline materials, the state of affairs becomes more complex as in a polycrystalline material there are numerous grains with various kinds of orientations and sizes. For each grain, slip can occur in its most favorably oriented slip system when the applied stress satisfies equation (2.39). But for the material to deform, the external stress must be at least large enough so as to be able to initiate the motion of dislocations in grains with the largest yield stress as given by equation (2.39). More over, the stress should also be large enough to enable the dislocations to cross the grain boundaries. This is one of the main reasons why polycrystalline materials are harder than their single-crystal counterparts. The theory also holds true for superlattices in which not only the grain boundaries in each individual layer but also the interfaces between layers play a similar role as grain boundaries do in a polycrystalline material.

The impediments of grain boundaries to the movement of dislocations can be attributed to two factors:

(1) The grain boundary is an area where atomic placement is irregular and as a result there is an interruption in the slip system;

(2) Two adjacent grains have different crystallographic orientations and therefore different slip systems. A dislocation which moves from one grain into another has to adjust its direction.

Thus it can be inferred that the more grains a material has, the more difficult for the dislocations to move. To put it in another way, the finer the grains are, the harder the material is. The yield stress of a polycrystalline material has been empirically related to the average grain size through the Hall-Petch equation[30]:

$$\sigma_y = \sigma_0 + k_y d^{-\frac{1}{2}} \tag{2.41}$$

where d is the average diameter of the grains; σ_0 and k_y are constants for a particular material.

Again, using equation (2.33), we obtain the hardness dependence on the average grain size:

$$H = H_0 + kd^{-\frac{1}{2}} \tag{2.42}$$

The above discussion can be extended to let d refer to the average spacing between any barriers to the dislocation movement instead of grain boundaries as in a polycrystalline material. In the case of superlattices, if the individual layer thicknesses are

comparable to the grain sizes, d can be identified with the superlattice periodicity Λ and thus we have the Hall-Petch relationship for the hardness of a superlattice:

$$H = H_0 + k\Lambda^{-\frac{1}{2}} \tag{2.43}$$

A more generalized model is to replace the ½ in the exponential part with a fractional variable f which can be determined for different superlattice systems using data fitting methods:

$$H = H_0 + k\Lambda^{-f} \tag{2.44}$$

The hardness of a superlattice is not only regulated by its periodicity, but is also modified by the elastic moduli difference between the two constituent materials. Materials with larger elastic moduli generally have stronger inter-atomic binding. It is more difficult for dislocations to form and move in these materials and therefore they exhibit greater hardness.

J. S. Koehler[4] proposed that enhanced hardness could be achieved by alternately layering two crystalline materials with different modulus of rigidity (shear modulus). Suppose the two constituent materials are represented by A and B with A having the smaller elastic modulus. According to Koehler's theory, to obtain enhanced hardness, the lattice parameters of A and B should be close enough to avoid large mismatch strains at the interface; their elastic moduli should differ as much as possible; the bonding between

the atoms of A and B should be large, i.e., of the same order as the bonding between two A atoms or two B atoms; and the thickness of each layer should be small (less than 100 atomic layers) so that dislocation generation cannot occur in layer A and dislocations generated in layer B won't pileup in layer A.

Using elasticity theory, Koehler derived the largest resolved shear stress a screw dislocation encountered from the nearest interface:

$$\sigma_r = \frac{RG_A \cos\alpha}{8\pi} \tag{2.45}$$

where $R = \frac{G_B - G_A}{G_B + G_A}$ with G_A and G_B the shear moduli (moduli of rigidity) of material A and B; α is the angle between the interface normal and the glide plane.

The increase in the yield stress as a result of this moduli modification is obtained by combining equation (2.45) with equation (2.39):

$$\sigma_G = \frac{\sigma_r}{\cos\alpha\cos\beta} = \frac{RG_A}{8\pi\cos\beta} \tag{2.46}$$

and the increase in hardness is obtained by applying equation (2.33):

$$H_G = \frac{3RG_A}{8\pi\cos\beta} \tag{2.47}$$

As an example, let us consider the Cu/Ni system. Both copper and nickel are fcc-structured crystals with slip systems consisting of the {111} planes and the <110> directions. The shear elastic moduli of copper and nickel are 4.6×10^4 Mpa and 7.6×10^4

Mpa[31], respectively, which give R = 0.246. Assume the superlattice interface is the (100) plane. The angle between the normal to the (100) plane and the slip direction (110) is $\beta = 45^{o}$, as shown in Figure 2.23.

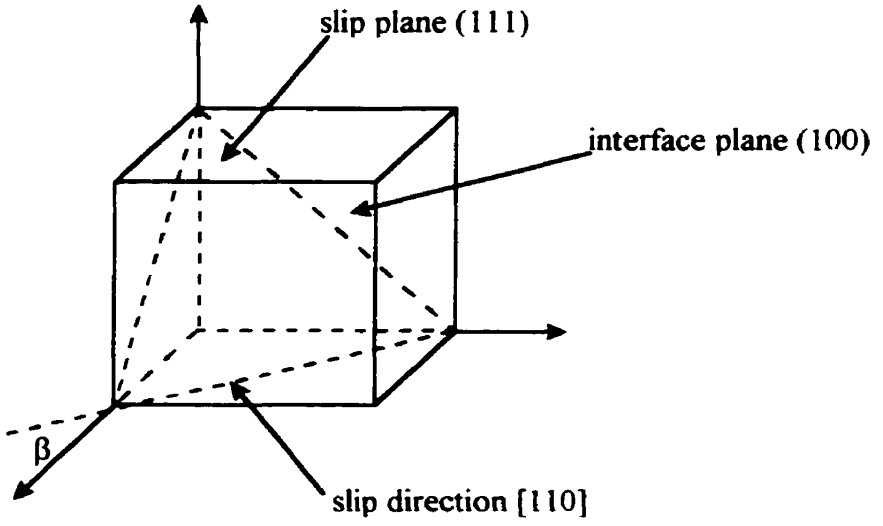

Figure 2.23: Orientation relationship between the interface and slip system in a Cu/Ni superlattice

Applying these values in equation (2.47) gives H_G = 1.9 Gpa. Therefore, an increase of about 2 Gpa in the hardness of a Cu/Ni superlattice can be expected as a result of the moduli modification.

In combination with equation (2.44), the total hardness of a superlattice can be characterized by three parts:

$$H = H_m + H_G + H_\Lambda \tag{2.48}$$

where H_G is the part from the moduli modification given by equation (2.47); H_Λ is the part resulting from periodicity modification, which is equal to $k\Lambda^{-f}$; and H_m is the part from the rule of mixture.

The rule of mixture value of the hardness of a superlattice is the weighted average (usually on the basis of volume) of the hardnesses of individual copper and nickel films. Suppose the thicknesses of layer A and B are l_A and l_B respectively, the rule of mixture value of the hardness of the A/B superlattice is given by:

$$H_m = \frac{l_A H_A + l_B H_B}{l_A + l_B} \tag{2.49}$$

In the case of equal thicknesses of the two layers, i.e., $l_A = l_B$, the rule of mixture value of the superlattice is simply the average of the hardnesses of the two materials:

$$H_m = \frac{1}{2}(H_A + H_B) \tag{2.50}$$

Chapter 3

Experimental

3.1 Electrodeposition process

The single bath used to produce the Cu/Ni superlattices is constructed using a three-electrode system as shown in Figure 3.1:

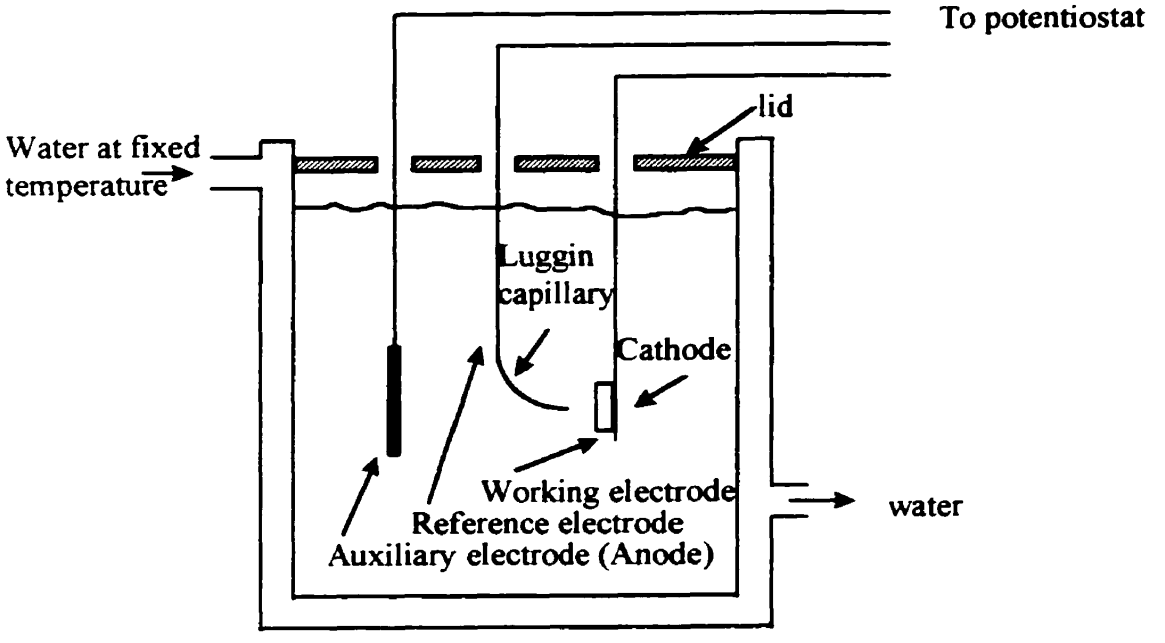

Figure 3.1: Schematic diagram of single bath for the Cu/Ni system

The auxiliary electrode is made of platinum which is both inert and highly conductive. This electrode serves as the anode for the cell. It is used actually as a source or sink of electrons for the chemical reactions taking place in the bath. It permits the transfer of electrons without itself being involved in the reactions.

The reference electrode is a saturated calomel electrode (SCE) which has a constant and stable potential of +0.268V[32] with respect to the standard hydrogen electrode (SHE). Its structure is shown in Figure 3.2:

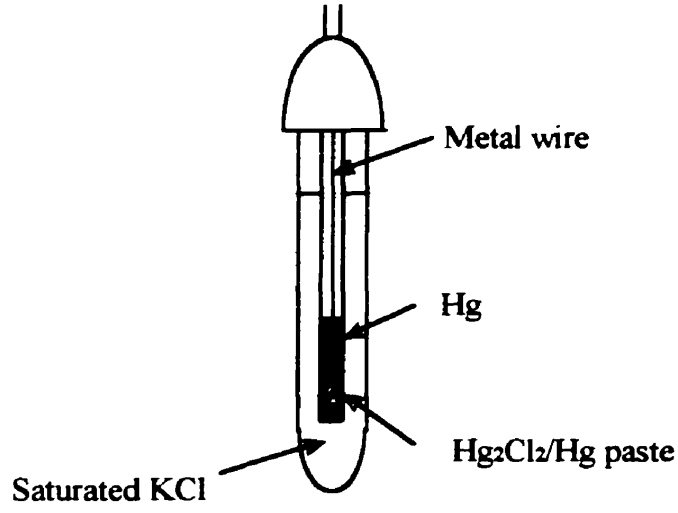

Figure 3.2: Structure of the saturated calomel electrode

The electrode is represented as $Hg|Hg_2Cl_2|Cl^-(aq)$ and the reaction at the electrode is:

$$Hg_2Cl_2 + 2e^- \rightarrow 2Hg + 2Cl^-, \quad E^0 = +0.268V \qquad (3.1)$$

The Hg_2Cl_2 salt has low solubility, as a result, the electrode potential is stable since it depends mainly on the activity of the Cl^- anions in the saturated KCl solution.

The working electrode is where the reduction reaction (deposition) takes place. It has a circularly-shaped cap with an opening in the center through which the substrate makes contact with the electrolyte solution. The diameter of the opening is 2.5cm and this defines the dimension of the superlattice sample that will be deposited. When preparing a sample, the substrate is made into a disk slightly larger in size than the opening of the cap and is pressed tightly inside the cap, making it in good contact with the electrode wire. The substrate used in this experiment is copper foil manufactured by Aldrich Chem. Co.. Its purity is 99.999% and its thickness is 0.025mm. It is polycrystalline with a (100) texture. The substrate is deoxidized in a 20% sulfuric acid solution for 30 seconds and rinsed in distilled water before use.

For electrodeposition, it is important to accurately control the potential of the working electrode. Therefore, the resistance between the working electrode and the reference electrode should be made as small as possible. This requires close positioning of the two electrodes and is realized with a Luggin capillary, a piece of glass into which the reference electrode is inserted and the tail of the glass is placed close to the working electrode as shown in Figure 3.1.

The contents of the electrolyte solution in this bath are given in Table 3.1:

Table 3.1 Composition of the Cu/Ni bath (1.2 liter)

Copper sulfate ($CuSO_4 \bullet 5H_2O$)	4.3g
Nickel sulphamate ($(H_2NSO_3)_2Ni \bullet 4H_2O$)	590g
Boric acid (H_3BO_3)	36g

The solution is composed this way such that it gives a copper concentration of 0.9g/l and a nickel concentration of 90g/l. This 1:100 ratio is made to keep the copper current sufficiently low during the short nickel deposition cycle, so the content of copper in the nickel layer is negligible (See section 2.2).

The bath is powered by a PAR (Princeton Applied Research) Potentiostat/Galvanostat Model 273 which in turn is controlled by a computer using the Headstart Creative Electrochemistry Software supplied by EG & G Instruments. The experimental setup is schematically shown in Figure 3.3:

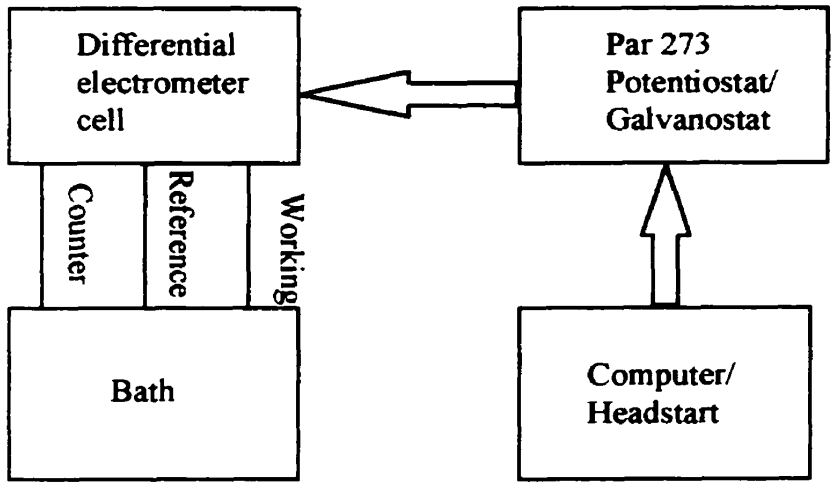

Figure 3.3: Experimental setup of electrodeposition

To program the potentiostat to control the deposition process, it is necessary to know the optimum potentials for depositing copper and nickel respectively. This is accomplished by sweeping the potential outputted from the PAR273 across a certain range and analyzing the change of the current in the bath. Figure 3.4a and 3.4b are the voltammograms obtained from the Cu/Ni bath as given in Table 3.1:

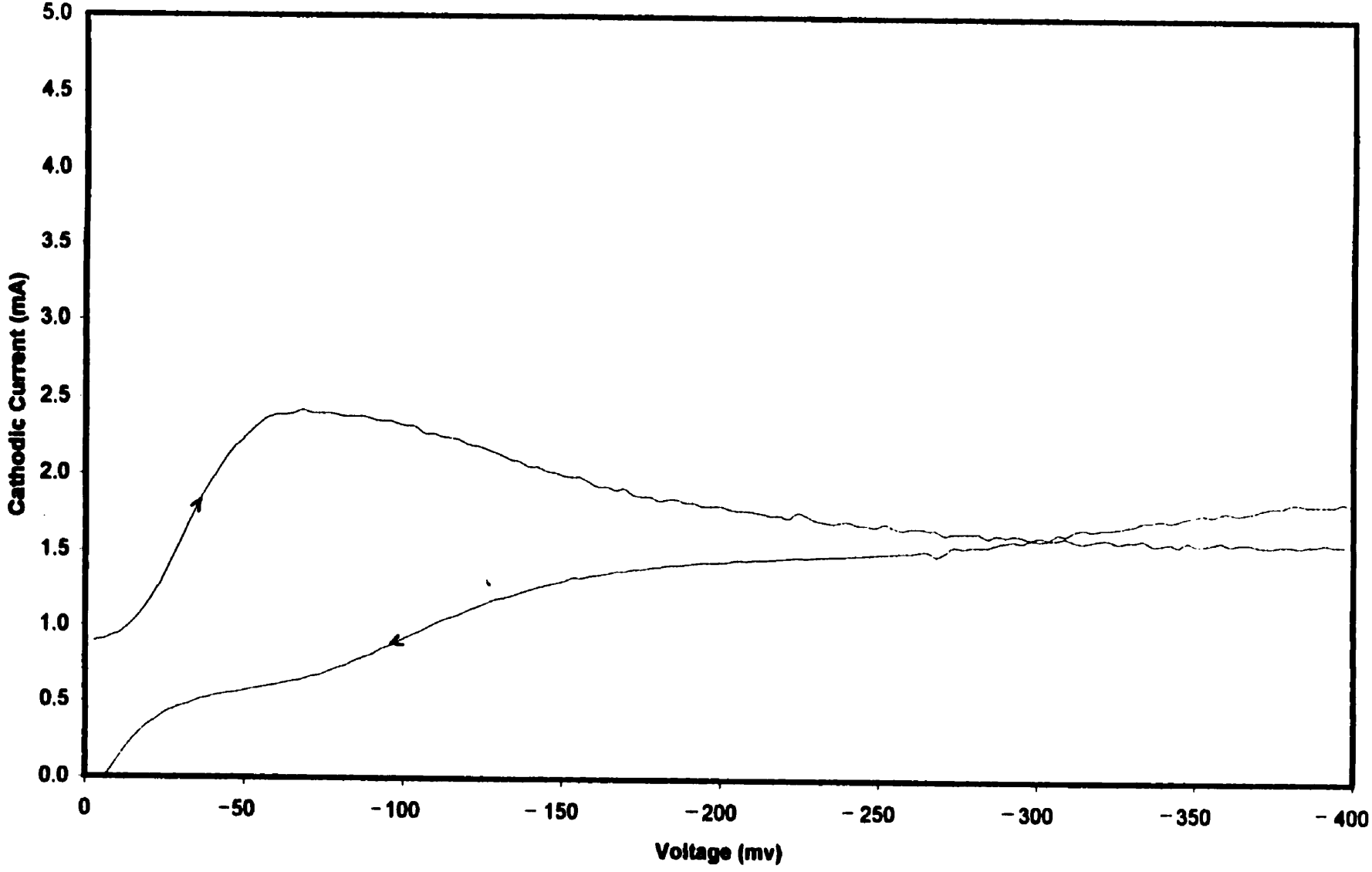

Figure 3.4a: Voltammetry diagram of the Cu/Ni bath in table 3.1

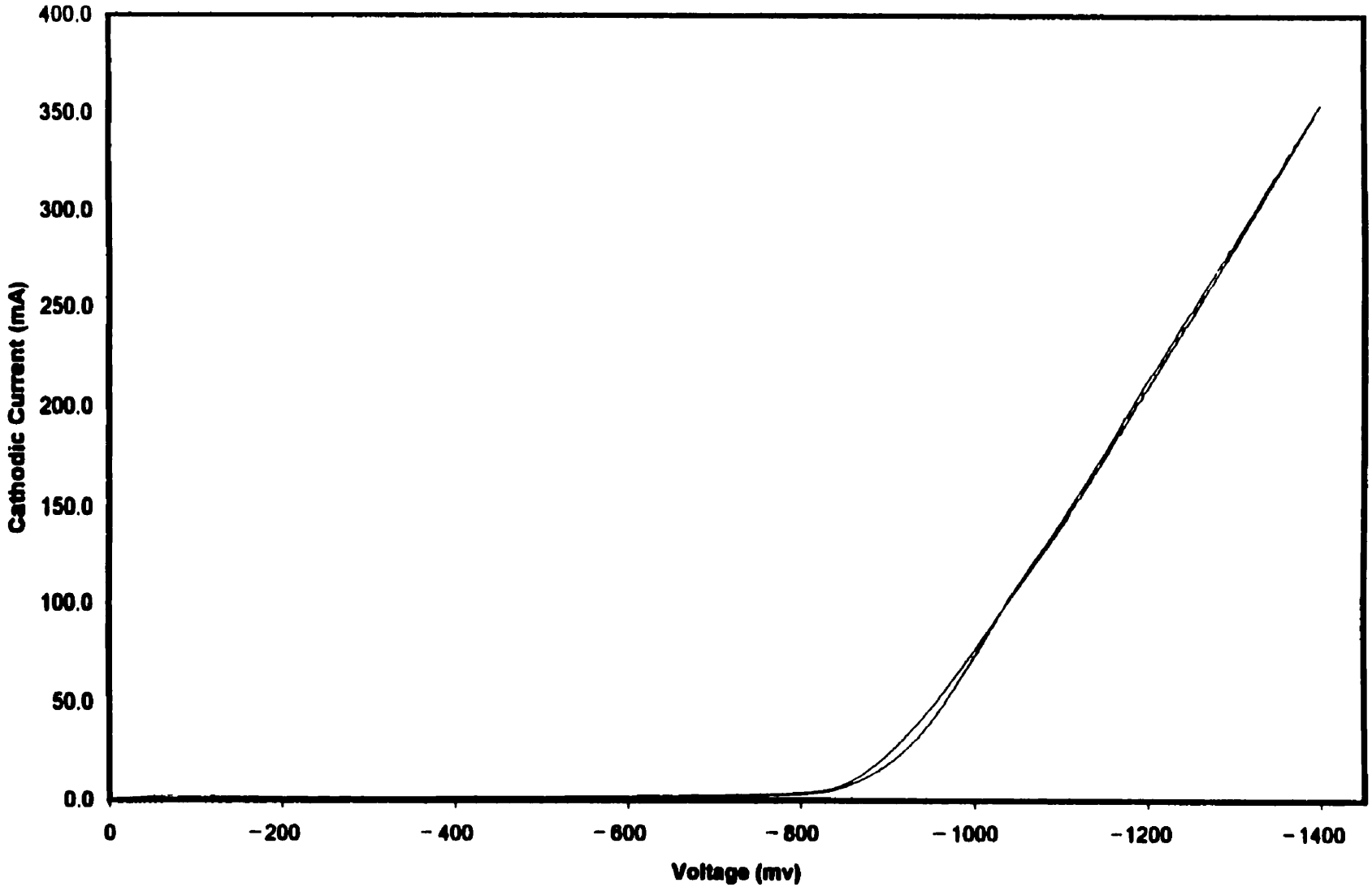

Figure 3.4b: Voltammetry diagram of the Cu/Ni bath in table 3.1

It can be seen from figure 3.4a that the current is rather small when the voltage between the reference electrode and the working electrode is below 800mv. Above 800mv, the current increases sharply. This is because copper is more noble than nickel and at low voltage only copper is deposited. As copper has a low concentration in the bath, the current from copper deposition is rather small as indicated in Figure 3.4b which uses a reduced vertical scale. When the voltage is increased to a certain level, nickel starts to deposit and, as nickel has a much higher concentration than copper, the current increases markedly. Therefore, in theory at least, the over-potential for depositing nickel can take any value lower than -800mv. We use -1190mv as the potential of the working electrode for nickel deposition in this experiment, which corresponds to a current of around 200mA. Similarly, from figure 2.4b we see that the copper current becomes stable after passing about -150mv, so we use -170mv as the potential of the working electrode for copper, which corresponds to a current of about 2mA. It should be noted that after the bath works for some time, the copper concentration may decrease a great deal and the current during copper deposition will drop accordingly, extending the time required to make a sample. Therefore, the copper content in the bath needs to be supplemented regularly.

Once the potentials for copper and nickel deposition have been determined, the PAR 273 can be programmed to generate the desired output to be applied to the bath. Table 3.2a and 3.2b contain two typical headstart programs for controlling the deposition of Cu/Ni superlattices:

Table 3.2a Headstart program for depositing Cu/Ni superlattices (Using one memory cell for a single data curve)

```
DCL
AR    1
AL    -5
MM    1       //Par 273 mode 1: potentiostat
MR    2
FP    0       //Starting point of data acquisition
LP    1023    //Last point of data acquisition; one memory for one layer
SCV   5
TMB   10078   //Time base, microsecond/per data
S/P   1
INITIAL   0     -680      //Starting point for copper: potential -170mv
VERTEX    991   -680      //Last point for copper
VERTEX    992   -4760     //Starting point for nickel: potential -1190mv
VERTEXT   1023  -4760     //Last point for nickel; mustn't exceed the LP value
ASM
DO 100;DCV 0; CELL 1;NC;TC;WCD;CELL 0;P 2;LOOP    //100 cycles (layers)
DO 100;DCV 1; CELL 1;NC;TC;WCD;CELL 0;P 2;LOOP
DO 100;DCV 2; CELL 1;NC;TC;WCD;CELL 0;P 2;LOOP
DO 100;DCV 3; CELL 1;NC;TC;WCD;CELL 0;P 2;LOOP
DO 100;DCV 4; CELL 1;NC;TC;WCD;CELL 0;P 2;LOOP
DO 100;DCV 5; CELL 1;NC;TC;WCD;CELL 0;P 2;LOOP    //Store a total of 6 curves
TRANSFER DATA FROM PSTAT
SAVE DATA & EXIT SETUP
```

Table 3.2b Headstart program for depositing Cu/Ni superlattices (Using three memory cells for a single data curve)

```
DCL
AR    1
AL    -5
MM    1
MR    2
FP    0          //Starting point of data acquisition
LP    3071       //Last point of data acquisition; three memories for one layer
SCV   3
TMB   11086
S/P   1
INITIAL    0     -680
VERTEX     3067  -680
VERTEX     3068  -4760
VERTEXT    3071  -4760
ASM
DO 500;DCV 0; CELL 1;NC;TC;WCD;CELL 0;P 2;LOOP    //500 cycles (layers);
DO 500;DCV 3; CELL 1;NC;TC;WCD;CELL 0;P 2;LOOP    //collect 2 curves in total
TRANSFER DATA FROM PSTAT
SAVE DATA & EXIT SETUP
```

The PAR 273 has 6 memories for data acquisition where each memory has a capacity of 1K bytes. The program in table 3.2a uses one memory (1K bytes) to store the data produced during the deposition of one double layer (one layer of copper and one layer of nickel). Therefore, data of a total of 6 double layers can be collected. The

program in table 3.2b uses three memories (3K bytes) to store the data of one double layer and as a result a total of 2 data sets can be collected.

The data acquired by PAR 273 during the deposition of a Cu/Ni superlattice is processed using software[33] developed by the author to produce a statistical diagram as shown in Figure 3.5.

The diagram shows the state of the current during the deposition of copper and nickel and the progress in the growth of their layer thicknesses. It may be used as the reference for programming the next sample.

The time base TMB is the time required for collecting one datum during the deposition process. It can be used to calculate the time for depositing one layer of copper or nickel. In the example of table 2.2a, 992 data (from 0 to 991) are collected during copper deposition, so the time for depositing one layer of copper is 992 x 10078 microseconds or 10 seconds. Similarly the time for depositing one layer of nickel is 32 (from 992 to 1023) x 10078 microseconds or 0.32 seconds. There is a 2-second pause after depositing one double layer, as indicated by the statement "P 2" in the "DO" lines, so the actual time for depositing a single double layer is (10 + 0.32 + 2) seconds or 12.32 seconds, and the total time for preparing a sample of 600 layers is therefore 12.32 x 600 seconds or 2 hours 4 minutes.

The time base TMB and the first and last points of copper and nickel cycles (INITIAL and VERTEX) are the most important parameters in a program. They can be determined as follows:

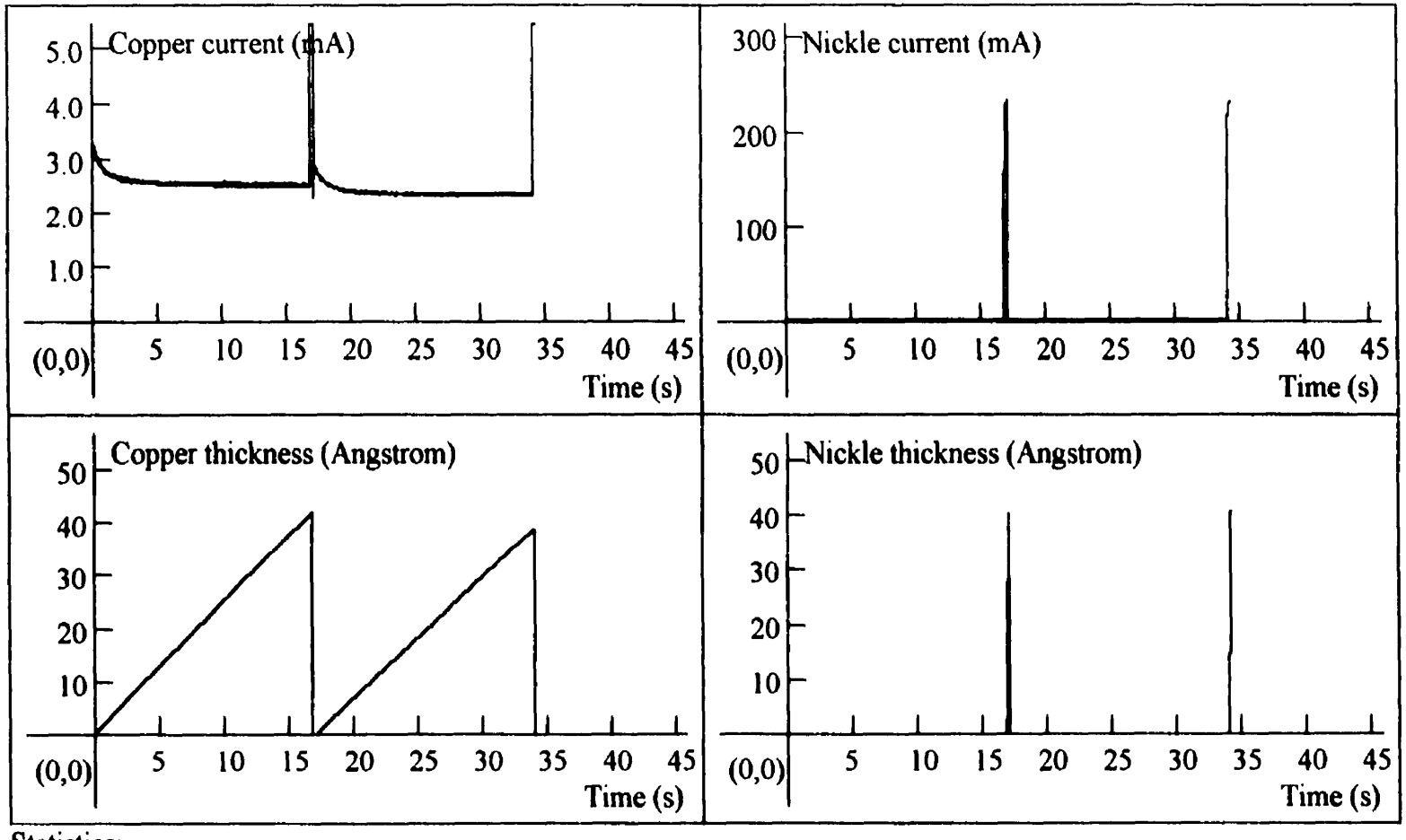

Statistics:

Cu reduction potential: -170.0 mv Ni reduction potential: -1190.0 mv

Cu deposition time/layer: 16.873080 s Ni deposition time/layer: 0.222600 s

Average Cu thickness/layer: 40.23 Angstrom Average Ni thickness/layer: 40.52 Angstrom

Figure 3.5: A sample Chrono-Amperometric diagram

First, use the program in table 3.2a to prepare a reference sample; process the data to obtain a diagram as the one shown in figure 3.5; use the statistics to calculate the times needed for depositing one angstrom of copper and one angstrom of nickel, letting them represented by t_{0Cu} and t_{0Ni}.

Next, design the copper and nickel layer thicknesses for the new sample, letting them be d_{Cu} and d_{Ni}. The time needed for depositing one layer of copper t_{Cu} is thus given by:

$$t_{Cu} = d_{Cu} t_{0Cu} \tag{3.2}$$

and the time for nickel t_{Ni}:

$$t_{Ni} = d_{Ni} t_{0Ni} \tag{3.3}$$

Suppose the number of memories used for collecting the data for one double layer is n, the time base is then given by:

$$TMB = \frac{t_{Cu} + t_{Ni} + 2}{1024 \times n \times 10^6} \tag{3.4}$$

The number of copper points is:

$$p_{Cu} = \frac{t_{Cu} \times 10^6}{TMB} \tag{3.5}$$

and the number of nickel points is:

$$p_{Ni} = \frac{t_{Ni} \times 10^6}{TMB} \tag{3.6}$$

Usually n is chosen to be either 1 or 3 which correspond to the programs in table 3.2 a and 3.2b respectively. The value of n is decided in a way such that the time base, TMB given by equation (3.4), is no less than 4000 microseconds and the number of nickel points given by equation (3.6) is no less than 20 for the consideration of the sensitivity of the PAR 273. Once a sample is prepared, its experimental parameters can be used as the reference for calculating the program parameters of the next one.

After the deposition is completed, the sample is rinsed and dried. For samples of several microns in thickness, they are capable of self-supporting and the substrate can be removed using the following solution:

Table 3.3 Solution for etching copper substrate

Water (H_2O)	9ml
Chromium trioxide (CrO_3)	5g
Sulfuric acid (H_2SO_4)	1ml

To prevent the samples from being damaged by the solution, they are covered with a thin layer of stop-off lacquer (Marivac Limited). The lacquer needs to be dried before the samples can be put into the etching solution and it can be removed using acetone when the etching is done.

3.2 X-Ray investigation of samples

A Ricagu model D/Max-1200 X-ray diffractometer is used to study the structure of the Cu/Ni multilayer samples. The anode (anti-cathode) is made of copper, which produces its characteristic x-ray radiation. The K_β radiation of Cu is absorbed by a nickel filter and the K_α is used as the working radiation. The K_α itself is actually a doublet which consists of $K_{\alpha 1}$ of 1.544 angstroms and $K_{\alpha 2}$ of 1.540 angstroms. The two wavelengths are so close to each other that the resulting broadening of the diffraction peaks is virtually invisible. The setup of diffractometer is shown in Figure 3.6.

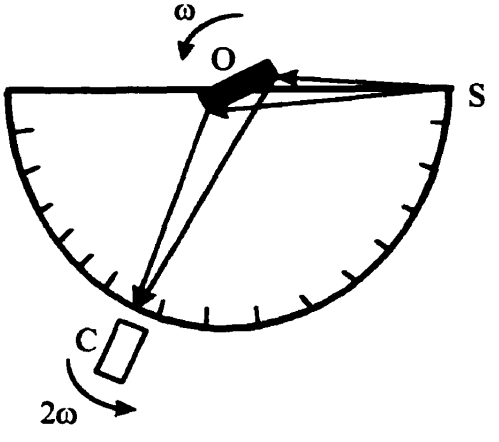

Figure 3.6: Schematic setup of the x-ray diffractometer
S: X-ray source; O: Object; C: Geiger-Muller counter

In Figure 3.6, the sample, the X-ray source and the detector are oriented such that the reflected beam and the incident beam are symmetrical about the normal of the sample surface. During a diffraction experiment, both the sample and the detector are rotating around a common axis so that the incident beam sweeps through a pre-chosen range of angles. This enables groups of planes with different orientations in the sample to satisfy the Bragg's law and be detected. To keep the previously defined geometrical orientations of the system, the detector rotates at an angular speed twice that of the sample, as is shown in Figure 3.7.

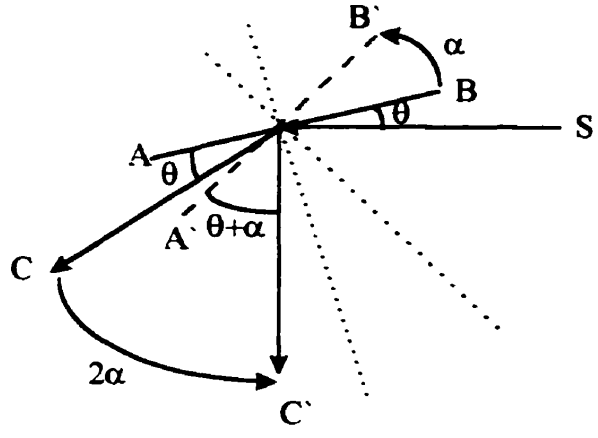

Figure 3.7: The sample AB rotates by an angle of α, the reflected the beam rotates by an angle of 2α.

3.3 Hardness test

Earlier hardness test was conducted by scratching one material against another[1]. A qualitative scale was devised to compare the relative hardness of some natural materials, thus talc has the lowest hardness of 1 and diamond the highest of 10 in the Mohs scale. Quantitative determination of hardness have been developed over the years and a number of techniques have been introduced to meet the requirements of different types of samples.

In general, all the tests are conducted by pressing an indenter into the surface of the sample under controlled conditions of load and rate of application. The depth or the size of the resulted permanent plastic deformation is measured and related to a hardness value by the formula:

$$H = \frac{F}{S} \tag{3.7}$$

where F is the load of force and $S = \pi a^2$ is the contact area as shown in Figure 3.8.

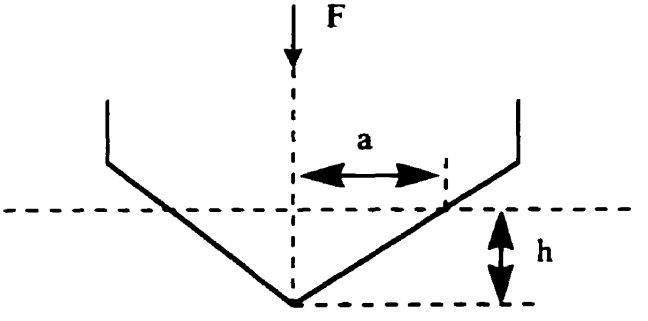

Figure 3.8: Indentation made by an indenter: a, contact radius; h, depth of penetration; F, load

For bulk materials, the loads are fairly large and the dimensions of the indentation can be easily identified.

For thin films, however, the loads applied are small, usually in the range of several μN to several mN, in order to avoid the influence of the substrate. The contact areas are too small to be easily observed. The interpretation of the dimensions of the indentations therefore requires special techniques. Nanoindenters, a variety of products now commercially available, provide a good method of nanoindentation characterization.

These instruments use a "depth-sensing" technique which keeps track of both the loads and the depths of the penetrations made by the diamond tip during the whole process of loading and unloading. The depths of penetrations are then converted to the contact areas using a theory developed by Doerner and Nix[34], and Oliver and Pharr[35]. Next the hardness is calculated using equation (3.7). This theory uses a polynomial expansion of the contact area as a function of the penetration depth. The function is usually determined by matching the contact area function at a range of depths of penetration to a homogenous, isotropic materials of known mechanical properties that are assumed to be constant with depths such as fused quartz.

As the impressions generated by the nanoindenters are rather small, it is important to take care in the preparation of the sample surface and the indentation process. A number of factors require special attention:

1. Specimen thickness:

The samples must be thick enough so as to prevent the impressions from showing through. Otherwise, the substrate on which the samples lies would have an effect on the measurement. The Cu/Ni samples investigated here have thicknesses of about 5 μm and therefore are about ten times the maximum depths of penetration made by the nanoindenters.

2. Relative positions of the impressions:

To obtain a hardness value of a sample as precise as possible, it is necessary to make several indentations to obtain an average value. However, the arrangement of the atoms will be distorted in the vicinity of an impression, so indentations should be made with proper separations. To minimize the influence of the nearby impressions, an

indentation should be made in a location at least three times the dimension of the indentations. The same separation should also be allowed between an impression and the edge of the sample.

3. Direction of the applied force:

The motion of the tip must be made perpendicular to the surface of the sample. Low readings would result if the tip penetrates the sample not in a right angle.

4. Rate and duration of the load:

Application of load should be slow in order to minimize inertial effect and give the sample time to respond to the load.

5. Flatness of the surface:

If the surface of the sample has a convex shape, a spring effect will be manifested and the readings would be low as a result of the spring resistance to the applied load. Therefore, samples whose surfaces are not flat should be placed on the substrate with the convex side down to eliminate this spring effect.

Chapter 4

Results

4.1 X-Ray diffractograms

Samples which were successfully striped off their substrates were subject to X-ray diffraction determination in order to verify the coherency of the interfaces and to determine their periodicities. The samples were scanned through a range of 40° to 60° in 2θ, which cover the (111), (200) and (220) orientations of the multilayers. The scanning angle increases by 0.02° each step and the scanning rate is 2 seconds per step. Typical X-ray diffractograms are presented in figures 4.1 and 4.2.

All the samples were grown on copper foils supplied by Aldrich Chem Co.. The foils are 99.999% in purity and 0.025mm in thickness. Figure 4.3 is the X-ray diffractogram of the copper substrate.

Samples which produced well-defined satellites were evaluated for their superlattice periodicities using equation (2.31). These data are presented in table 4.1, together with the programmed Cu/Ni thicknesses and the outputted data from Par273 for comparison.

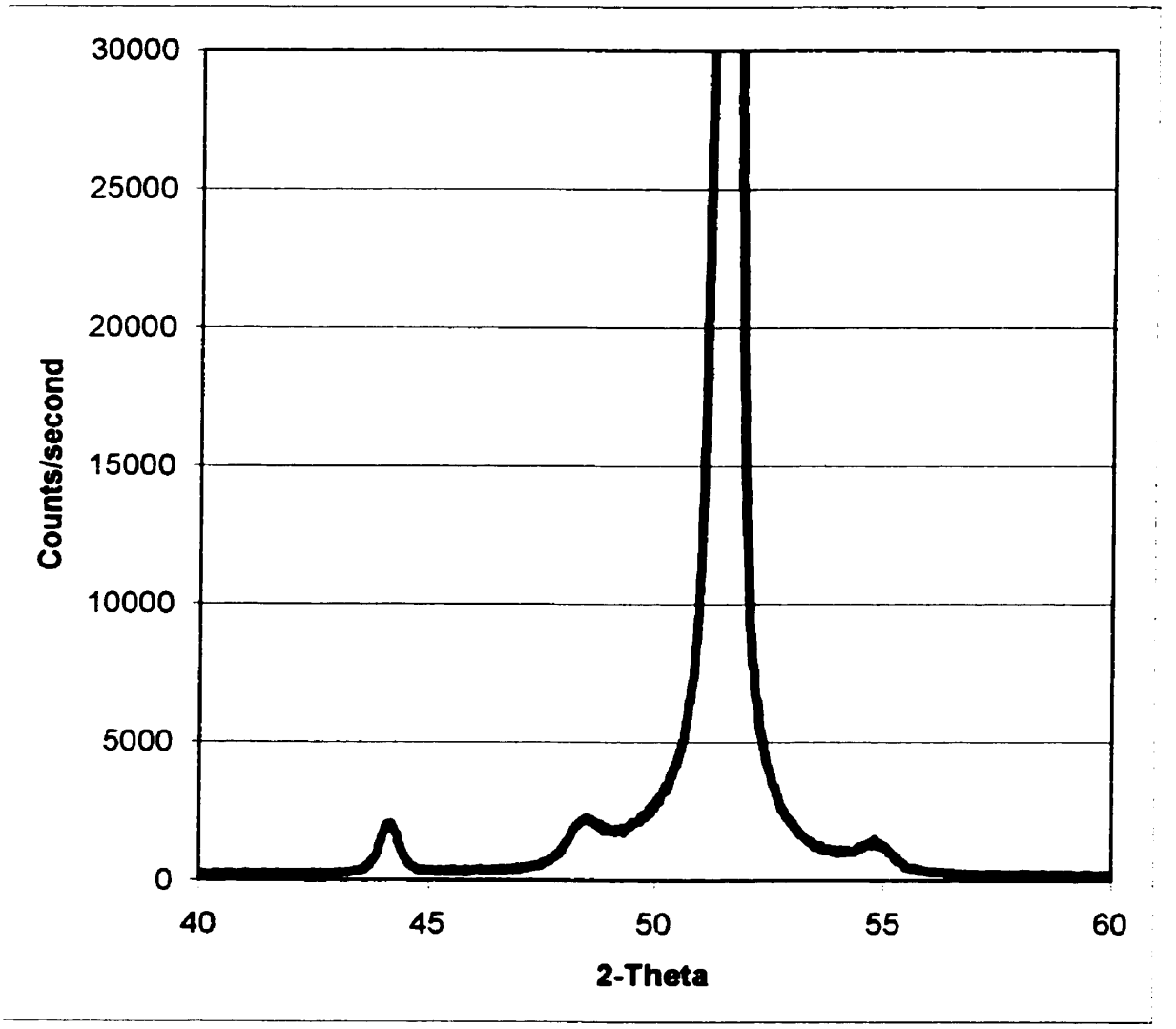

Figure 4.1: X-ray diffractogram of Cu/Ni multilayer sample
(Cu thickness: 10.5 angstroms; Ni thickness: 11 angstroms)

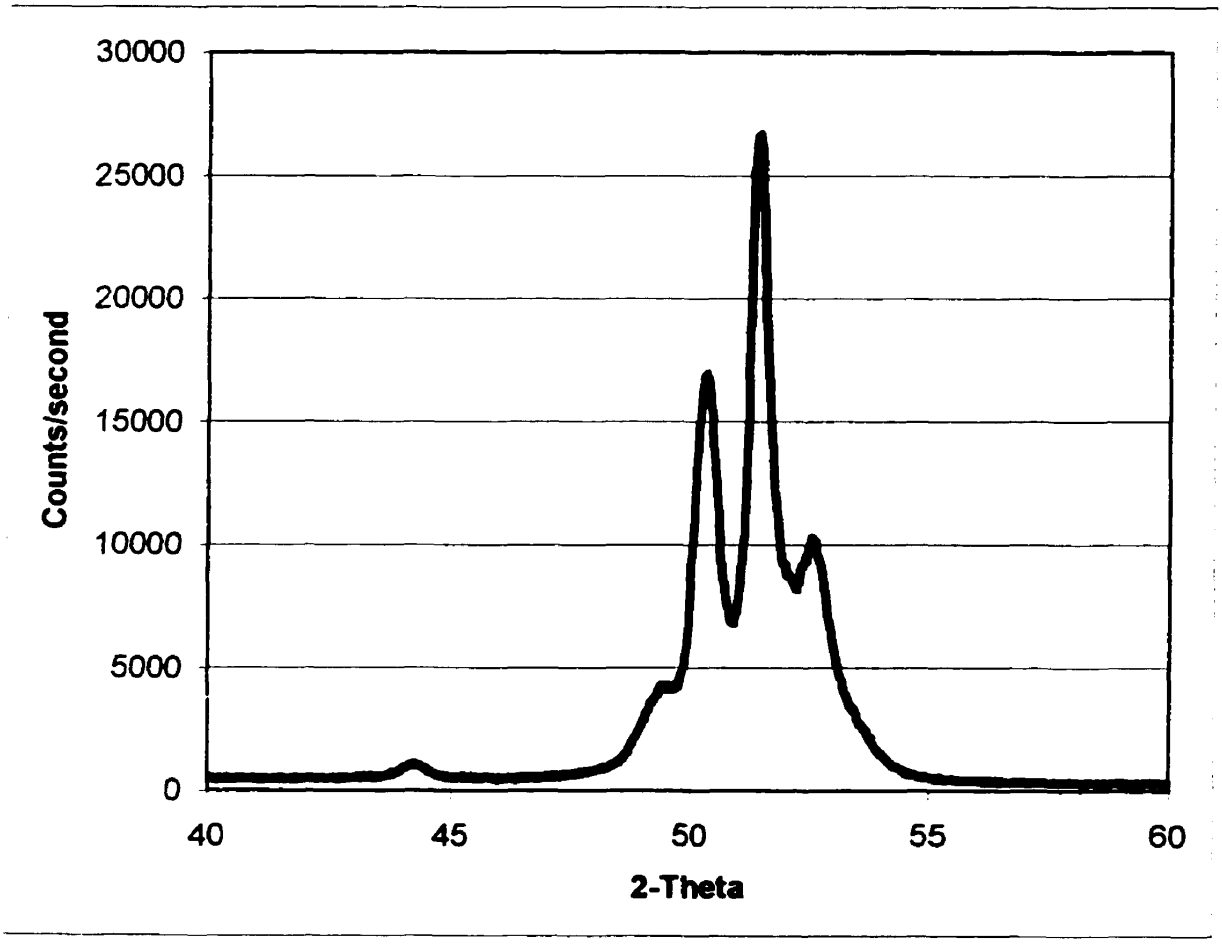

Figure 4.2: X-ray diffractogram of Cu/Ni multilayer sample
(Cu thickness: 40.2 angstroms; Ni thickness: 40.5 angstroms)

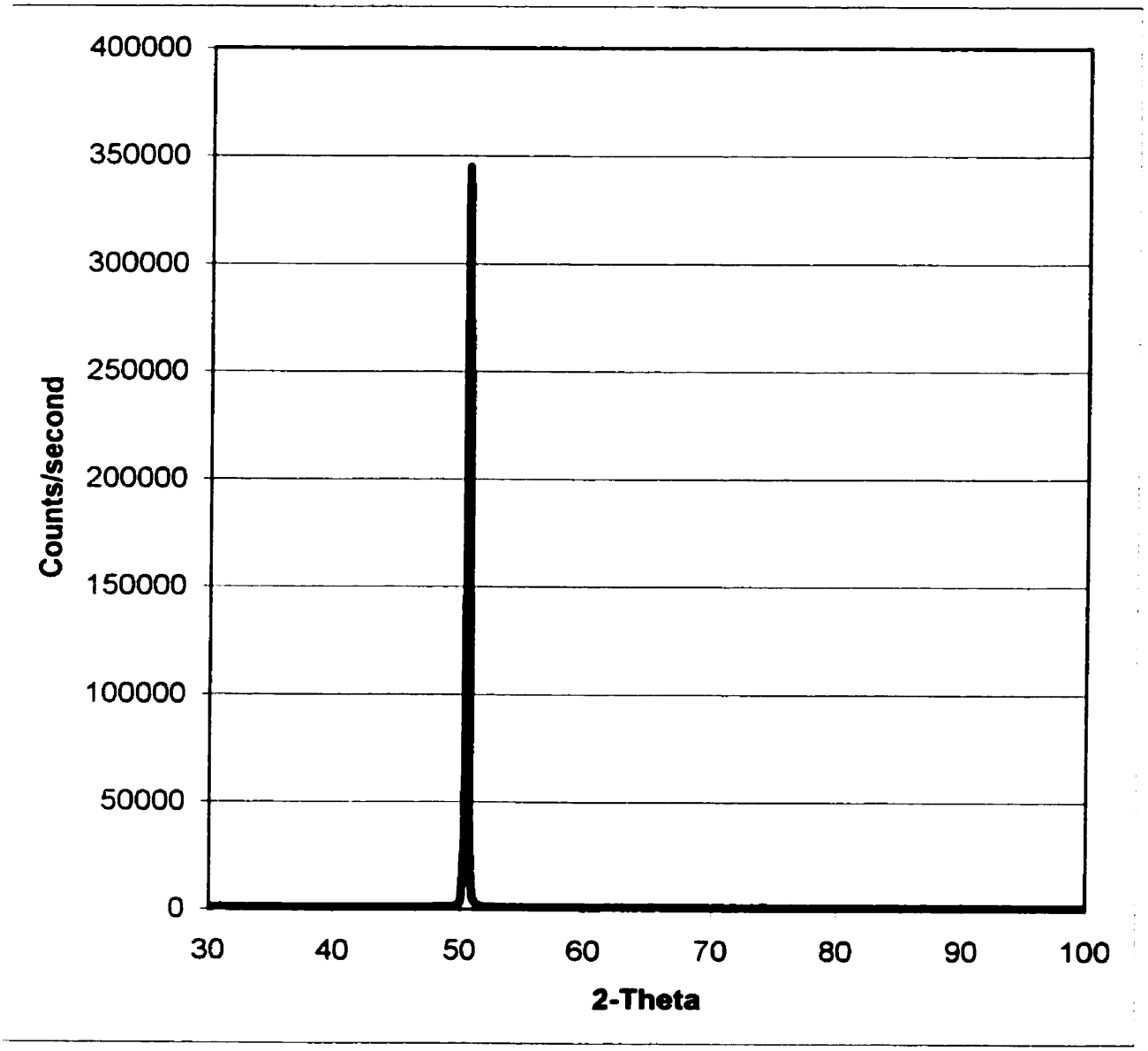

Figure 4.3: X-ray diffractogram of copper substrate
(Aldrich Chem Co.. Purity: 99.999%; thickness: 0.025mm)

Table 4.1 Comparison of superlattice periodicities from X-ray diffractograms, experimental output from Par273 and programmed values
(All units in Angstroms)

		#1	#2	#3	#4	#5	#6
Programmed	Cu thickness	10	20	30	40	50	60
	Ni thickness	10	20	30	40	50	60
	Periodicity	20	40	60	80	100	120
Output from Par273	Cu thickness	10.5	17.8	27.1	40.2	46.2	60.8
	Ni thickness	11	20	33.4	40.5	51.7	65.4
	Periodicity	21.5	37.8	60.5	80.7	97.9	126.2
X-Ray diffraction	Periodicity	30.6	41.2	68.5	83.8	96.3	115.1

4.2 Hardness results

Samples which exhibit well-defined satellites were subject to hardness tests. The Cu/Ni multilayers in this work were characterized on a Hysitron TriboScope and a CSIRO UMIS2000 nanoindenter. Both use a Berkovich diamond tip which has a triangular pyramid shape, and software which processes and analyzes the load and penetration depth data acquired during the indentation processes. Hardness values are outputted directly by

the software. The software also produces loading and unloading curves, and the hardness-depth curves as presented in figure 4.4 to 4.7 for several samples.

About five to ten indents were made on each sample at loads ranging from a few μN to several mN. The hardness values at the maximum penetrations of these indents were averaged and used to characterize the hardness of the samples. Measurements results which are too distant in value from the average are left out by the software in the averaging.

Three groups of samples were investigated for their hardness characteristics.

The first group of samples had equal copper and nickel thicknesses but varying periodicities. The average hardness values of these samples are presented in table 4.2. This table also contains the hardness values measured on pure copper and pure nickel thin films electro-deposited from the same bath used for the multilayer samples for comparison. These hardness values are presented in figure 4.8 as hardness versus superlattice periodicity and in figure 4.9 as hardness versus the inverse of the square root of the superlattice periodicity, the Hall-Petch plot.

Table 4.2 Measured hardness values of Cu/Ni multilayer systems and pure copper and nickel films

Sample	Cu	Ni	#1	#2	#3	#4	#5	#6
Hardness (Gpa)	0.82	2.5	4.4	5.6	4.4	3.0	2.6	0.84
Standard error (Gpa)	0.06	1.1	0.5	0.3	0.5	0.4	0.3	0.3

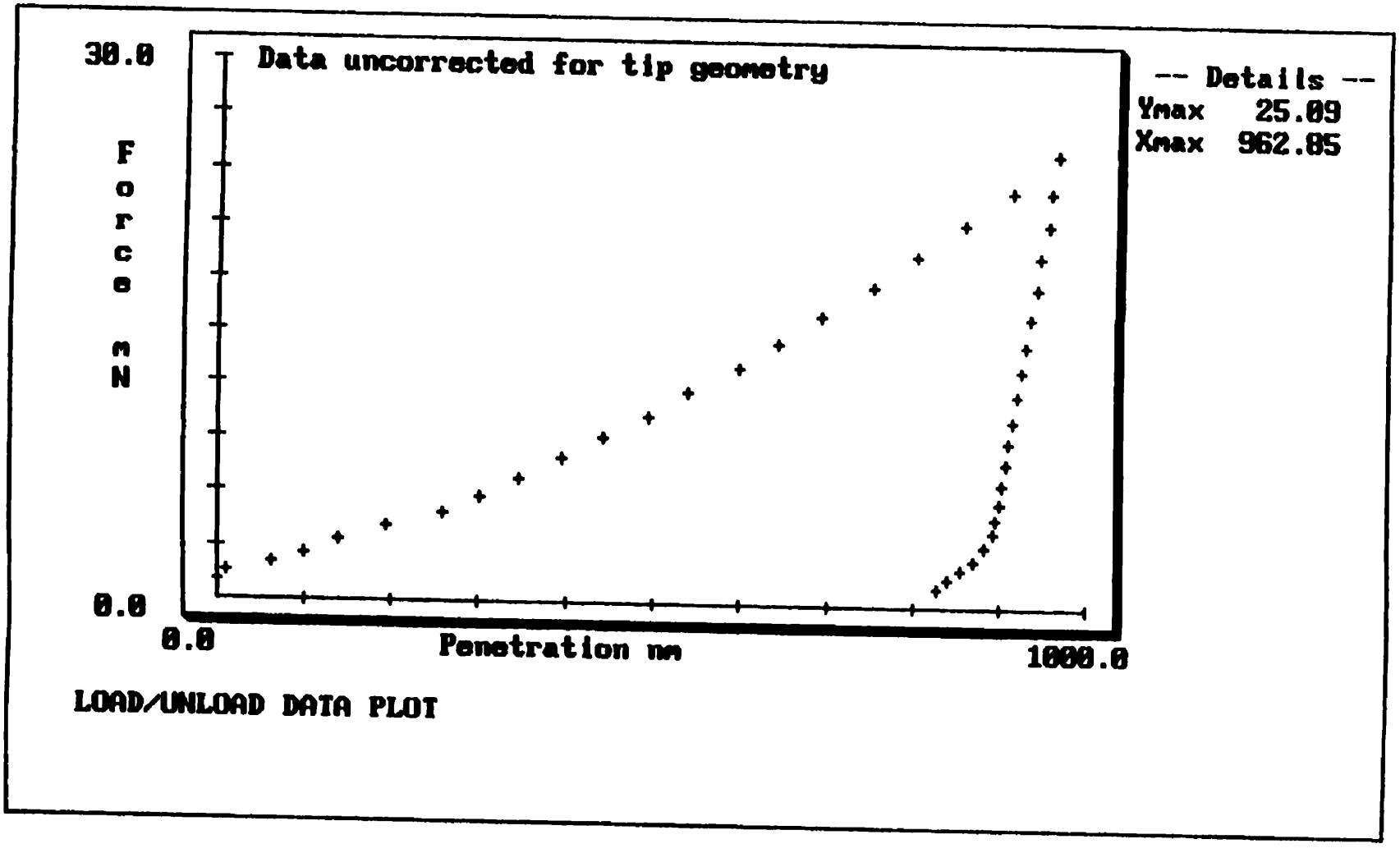

Figure 4.4: Load and unloading curve of pure copper

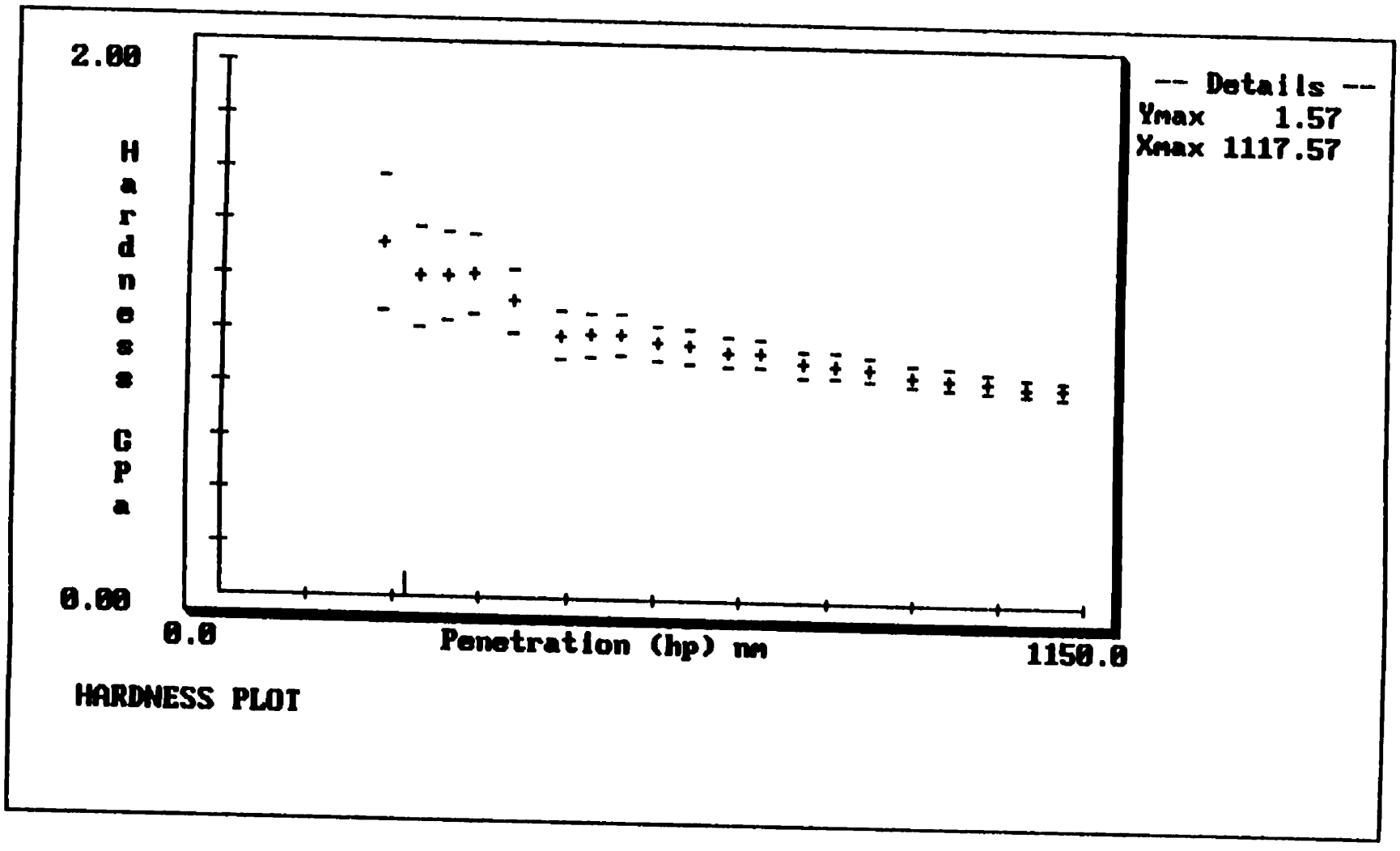

Figure 4.5: Hardness measurement curve of pure copper

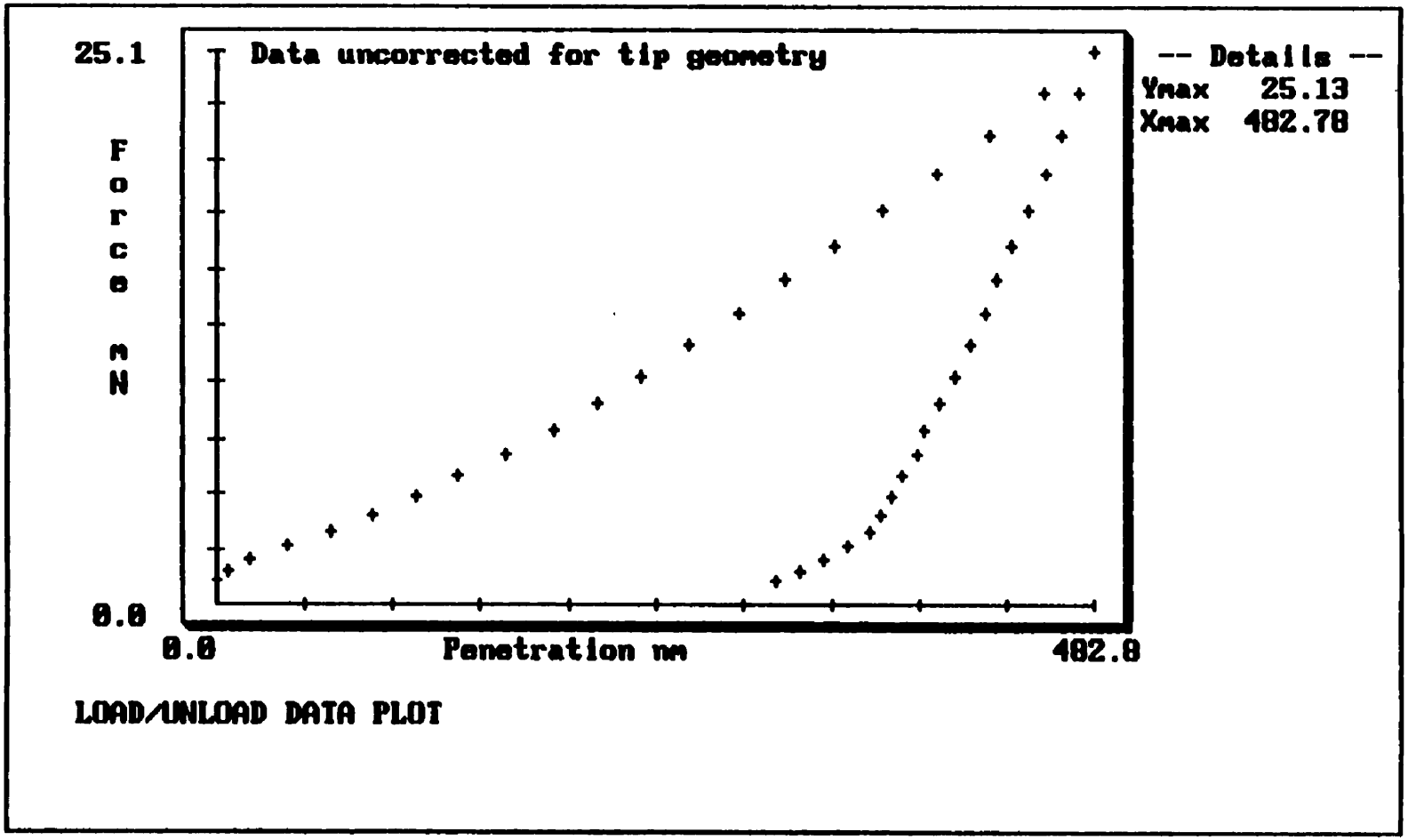

Figure 4.6: Load and unloading curve of Cu/Ni (periodicity: 83.4 angstroms)

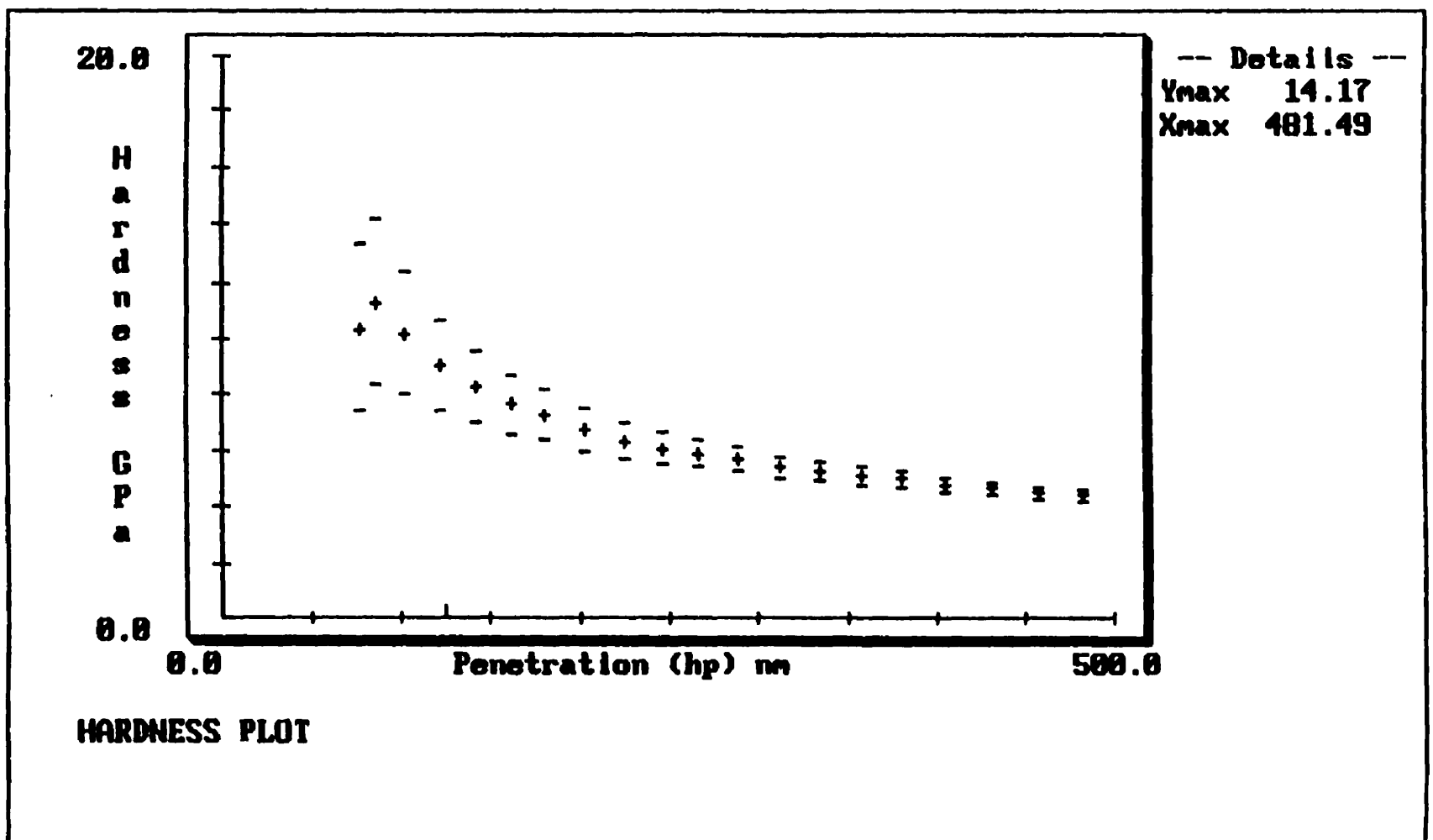

Figure 4.7: Hardness measurement curve of Cu/Ni (periodicity: 83.4 angstroms)

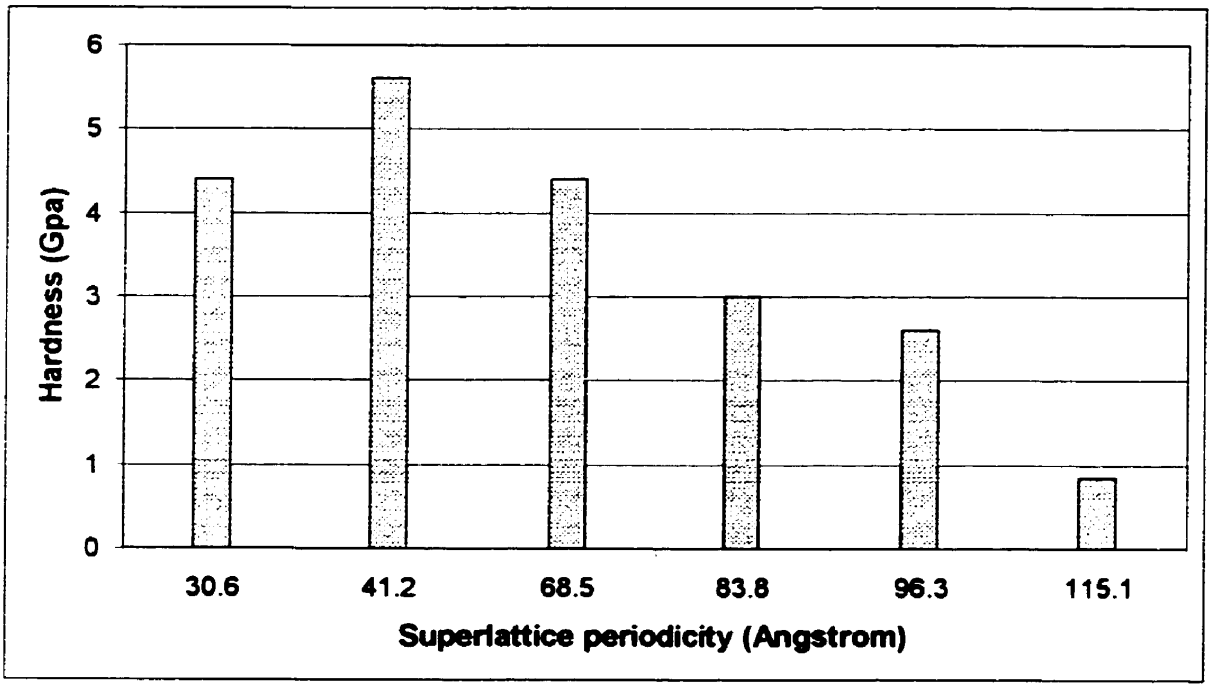

Figure 4.8: Hardness-superlattice periodicity plot

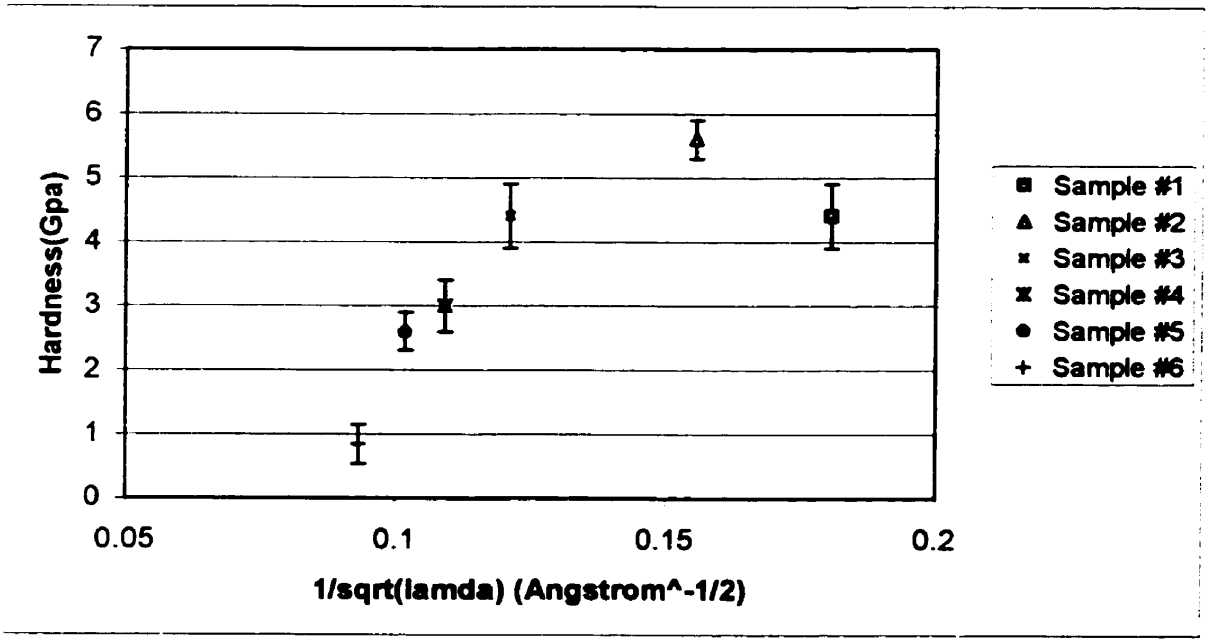

Figure 4.9: Hall-Petch plot of hardness values of Cu/Ni multilayers

The second group of samples had copper thicknesses kept fixed at about 10 angstroms while the nickel thicknesses varied. Data of the samples and the hardness dependence on the nickel thickness are presented in Table 4.3 and Figure 4.10.

Table 4.3 Sample thicknesses and hardness values
(All thicknesses in angstroms; hardness and standard error in Gpa)

Sample #	Cu thickness	Ni thickness	Periodicity	Hardness	Error
#7	8	17	27.6	5.3	0.4
#8	10	35	48.3	4.2	0.2
#9	9.5	41.4	50.9	3.9	0.1

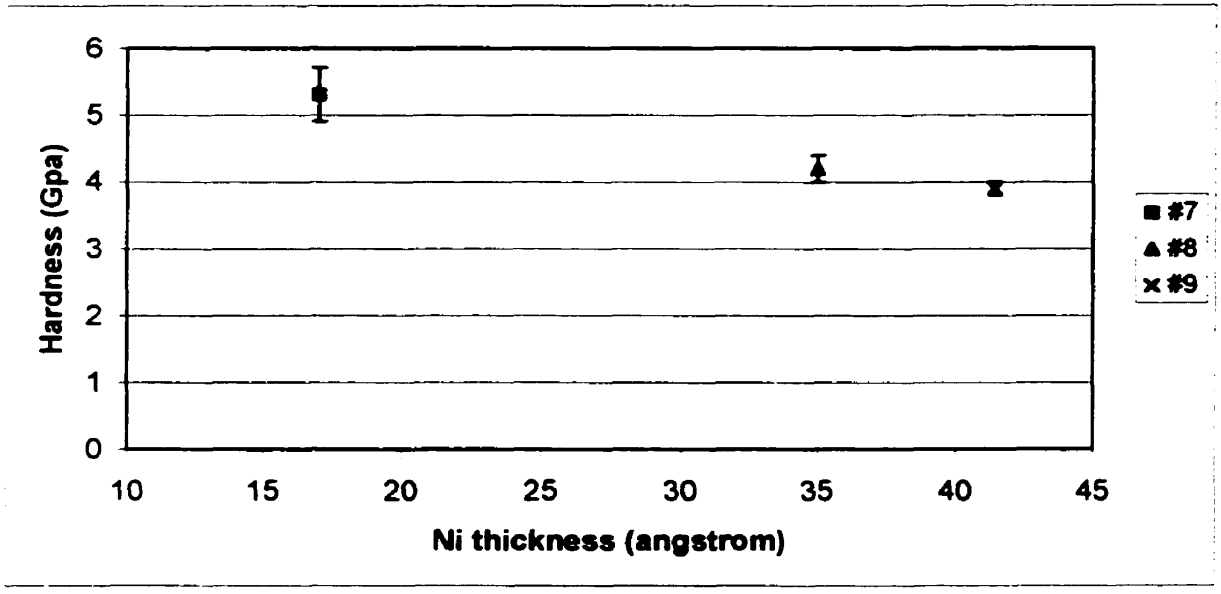

Figure 4.10: Hardness dependence on nickel thickness (Copper thickness ≈ 10 angstroms)

The third group of samples had nickel thicknesses fixed at about 50 angstroms while copper thicknesses change. The results of this group of samples are presented in Table 4.4 and Figure 4.11.

Table 4.4 Sample thickness and hardness values
(All thicknesses in angstroms; hardness and standard error in Gpa)

Sample #	Cu thickness	Ni thickness	Periodicity	Hardness	Error
#10	16.6	50.9	67.5	4.2	0.2
#11	25.9	56.3	82.2	4.0	0.5
#12	32.2	55.8	88	4.5	0.3
#13	22.6	45.8	68.4	4.2	0.4

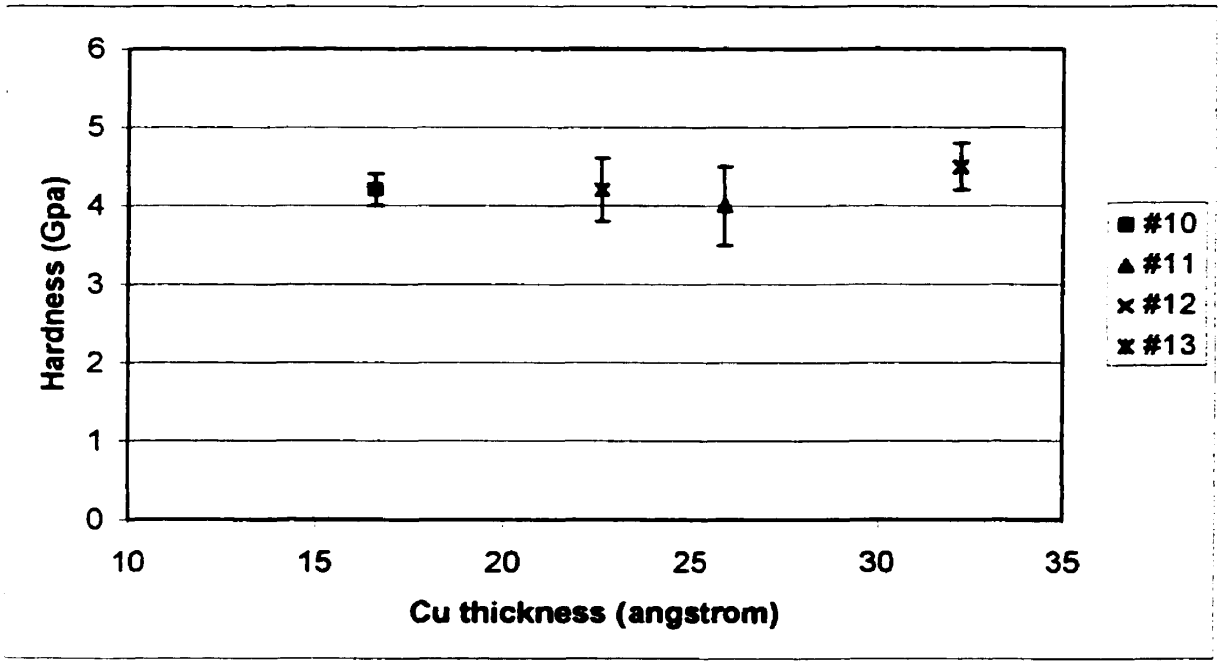

Figure 4.11: Hardness dependence on copper thickness (nickel thickness ≈ 50 angstroms)

Chapter 5

Discussions

5.1 X-Ray diffraction

X-ray diffraction shows that the Cu/Ni multilayer systems prepared by electro-deposition possess well-defined layered structures. This is proved by the appearance of satellite peaks surrounding the main Bragg peaks as shown in figure 4.1 and 4.2, which exhibit different copper and nickel thicknesses and ratios. The main Bragg peaks appear at an angle 2θ of around 51 degree which fall in between the (200) Bragg peaks of copper (50.4 degree) and nickel (51.8 degree). Figure 4.3 is the diffractogram of a copper substrate on which the multilayer samples were grown. It shows a strong (200) texture, indicating that the Cu/Ni multilayer systems grew epitaxially on the substrate.

Using the angular positions of the satellites, the superlattice periodicities of the samples were calculated with equation (1.31). Table 4.1 shows that there are differences in the copper and nickel thicknesses and the superlattice periodicities among the programmed values, the output values from the Par273 Potentiostat and the values obtained from the X-ray diffractograms. These differences can be attributed to the fluctuations in the bath compositions and the working conditions such as temperature instabilities. Also, the values from Par273 were calculated on the assumption that the deposition efficiency is 100 percent. Another fact is that the Par273 values were sampled only on a few layers during the deposition process which usually had hundreds or even thousands of layers grown. The superlattice periodicities obtained by X-ray diffraction are

more accurate and therefore are used in the analysis of the hardness variations with the superlattice periodicities.

5.2 Hardness results

As predicted by theory, hardness enhancement is found in the electro-deposited Cu/Ni multilayer systems. Figure 4.8 shows that hardness varies with superlattice periodicity. The maximum hardness occurs at a periodicity of around 41 angstroms in this group of samples. The values drop when the superlattice periodicities either increase or decrease from this point.

The maximum hardness, as measured, is 5.6 Gpa with a standard deviation of ± 0.5Gpa. This is more than twice the hardness of the nickel film deposited in the same bath and more than two times an increase over the rule-of-mixture hardness value H_m of copper and nickel alloy. As the volume ratios between Cu and Ni in the samples are approximately 1:1, the hardness value by rule-of-mixture is therefore the average of the two constituent materials. From table 4.2, we have:

$$H_m = \frac{H_{Cu} + H_{Ni}}{2} = \frac{0.82 + 2.5}{2} \approx 1.7(Gpa) \qquad (5.1)$$

The standard deviation in the rule-of-mixture value is:

$$\delta H_m \approx \pm 0.5 Gpa \qquad (5.2)$$

In section 2.4, equation (2.48) gives the hardness prediction for a Cu/Ni multilayer system. It consists of three parts: the rule-of-mixture contribution H_m, the elastic moduli modification contribution H_G and the superlattice periodicity contribution H_Λ. Using the result of equation (5.1), we have:

$$H = H_m + H_G + H_\Lambda = 1.9 + 1.7 + H_\Lambda = 3.6 + H_\Lambda \qquad (5.3)$$

The results presented in table 4.2 and figure 4.8 show that the samples with superlattice periodicities of 30.6, 41.2 and 68.5 angstroms exhibit hardness values greater than the combination of values from rule-of-mixture and elastic moduli modification. The other samples failed to show hardness values as large as predicted by equation (5.3). This may be explained as follows:

First, the elastic moduli modification model established by Koehler[4] assumes that the interfaces between the alternating layers of the superlattices are perfectly smooth and abrupt. This is not possible to achieve in the case of real multilayer systems. As a matter of fact, the interfaces in real multilayer systems have an intermixed region of the order of several angstroms[1]. Thus, there is actually a moduli gradient at the interfaces instead of an abrupt change. This lowers the hardness as predicted by equation (2.45).

Second, diffusion of the two materials into each other in the vicinity of the interface is also responsible for drop in the hardness values in the lower range of the superlattice periodicity. As the two layers become so inter-diffused, in cases where the superlattice periodicity nears 20 angstroms the superlattice effect greatly diminishes. This

is also partly the reason for some difficulties in the preparation of samples with small periodicities.

Third, the decrease of hardness in the larger range of superlattice periodicities may also be attributed to the motion of dislocations within individual layers[14]. Before the applied stress is large enough to drive the dislocations to cross the interface barriers, the dislocations may already move within the individual layers if the layer thickness is large. This will result in a lower measurement of hardness value.

The effect of the superlattice periodicity modification can be illustrated by a Hall-Petch type plot which gives hardness values versus the inverse of the square root of the superlattice periodicities as presented in figure 4.9. The plot shows that for the superlattice periodicity range of from about 40 to 80 angstroms, the hardness is roughly in linear relationship with the inverse of the square root of the superlattice periodicity. This is in agreement with theoretical prediction (section 2.4) and reports from other authors[12].

It should be noted, however, that the Hall-Petch relationship was first derived for polycrystalline materials[32][33]. It has then been extended to account for multilayer systems. Although there have been attempts at experimental confirmations of this theory, its validity remains to be further studied.

Figure 4.10 and figure 4.11 show some interesting trends in the hardness characteristics of superlattices.

When copper thickness is fixed at about 10 angstroms, hardness drops when nickel thickness increases from 17 angstroms to 41 angstroms. On the other hand, hardness basically remains constant when nickel thickness is fixed at about 50 angstroms while copper thickness varies from 16 to 32 angstroms.

This can be explained by the propagation of dislocations across the interfaces. There are two types of cross-interface motions of dislocations. One is from the lower elastic modulus layer of copper into the higher elastic modulus layer of nickel. The nickel layer has a higher strain energy and therefore dislocations in the copper side will encounter a repulsive force which is proportional to the moduli difference as is reflected in equation (2.45). When the nickel layer thickness is fixed, the number of dislocations which can move across the interfaces is mainly determined by the elastic moduli difference and is independent of the copper thickness. Therefore the hardness remains basically constant.

The other cross-interface motion of dislocations is from the nickel layer to the copper layer. As the strain energy in the copper layer is smaller than that in the nickel layer, the dislocations in the nickel layer can be easily driven into the copper layer. The number of dislocations which will propagate across the interface is in proportion to the number of dislocations in the nickel layer which in turn depends on the thickness of the nickel layer.

It should be noted that the hardness characteristics of superlattices are determined by many factors which are still not fully understood. A number of theoretical models have been proposed in an effort to explain results obtained in some experiments. A more accurate and complete model is yet to be developed to give a more satisfactory explanation to the hardness enhancement mechanisms of superlattice systems. Also, a more accurate and standardized hardness characterization system is desired to provide better experimental data in the hardness studies of superlattice systems.

Chapter 6

Conclusions

It has been proven once again by this work, that Cu/Ni multilayer systems may be produced using electrodeposition from a single bath. The samples posses well-defined layered structures with quite smooth interfaces as confirmed by X-Ray diffraction. By controlling the experimental conditions, the thicknesses of the individual copper and nickel layers can be tailored to meet desired requirements for the investigation of certain unique properties of superlattice systems.

The Cu/Ni systems exhibit enhanced hardness over both pure nickel or copper and the rule-of-mixture values of copper and nickel alloys. An increase in the maximum of hardness by a factor of 2 can be realized in the multilayer systems. Also, a Hall-Petch type relationship between hardness and superlattice periodicity is identified for the range of about 40 to 80 angstroms.

When nickel thickness is fixed at about 50 angstroms, hardness basically remains constant when copper thickness varies from about 16 to 32 angstroms. On the other hand, when copper thickness is fixed at about 10 angstroms, hardness drops when nickel thickness increases from about 17 to 41 angstroms.

In summary, electrodeposition methodology presented in this work appear to be efficient to produce good quality metal superlattice systems with special mechanical properties and thus has the potentials of being further exploited for both research purposes and industrial applications.

References

1. Scott Barnett and Anita Madan, Physics World, January, 45, (1998)

2. David Bradley, New Scientists, 20 march, 22, (1993)

3. A. Y. Liu and M. L. Cohen, Phys. Rev. B, 41, 10727, (1990)

4. J. S. Koehler, Physical Review B, Vol. 2, N0. 2, 15 July, 547, (1970)

5. Danko Simunovich and M. Schlesinger, J. Electrochem. Soc., Vol. 141, No. 1, January, L10, (1994)

6. William D. Sproul, Science, Vol. 273, 889, (1996)

7. R. C. Cammarata, Thin Solid Films, 240, 82, (1994)

8. B. J. Daniels, W. D. Nix and B. M. Clemens, Thin Solid Films, 253, 218, (1994)

9. T. E. Dinan and H. Y. Cheh, J. Electrochem. Soc., Vol. 139, N0. 2, February, 410, (1992)

10. T. Tsakalakos and J. E. Hilliard, J. Appl. Phys. 54 (2), February, 734, (1983)

11. Dong Li, Xi-Wei Lin and Shang-Cong Cheng, Appl. Phys. Lett., Vol. 68, No. 9, 26 February, 1212, (1996)

12. R. C. Cammarata and T. E. Schlesinger, Appl. Phys. Lett. 56 (19), 7 May, 1862, (1990)

13. R. F. Bunshan, R. Nimmagadda and H. J. Doerr, Thin Solid Films, 72, 261, (1980)

14. Xi Chu and Scott A. Barnett, J. Appl. Phys., 77 (9), 1 May, 4403, (1995)

15. Scott A. Barnett, Physics of Thin Films, 17, 2, (1993)

16. Scott A. Barnett, Annual Review of Materials Science, 24, 481, (1994)

17. C. A. Ross, Annual Review of Materials Science, 24, 159, (1994)

18. Ludimila Eckertova, Physics of Thin Films, Plenum Press, 96 (1986)

19. Blum W. 1921. Trans. Am. Electrochem. Soc. 40: 307-20

20. Tench DM, White JT. 1984, Metal Trans. A 15A: 2039-40

21. Yahalom J, Zadak O. 1987, J. Mater. Sci. 22: 499-503

22. Robert A. Alberty, Robert J. Silbey, Physical Chemistry, John Wiley & Sons, Inc., 243, 1992

23. Marcel Pourbaix, Atlas of Electrochemical Equilibia in Aqueous Solutions, NACE Cebelcor, 1974

24. S. G. Bratsch, J. Phys. Chem. Ref. Data 18:1(1989)

25. Peter Luger, Modern X-Ray Analysis on Single Crystals, W de G, 80, 1980

26. Harold P. Klug & Leroy E. Alexander, X-Ray Diffraction Procedures, John Wiley & Sons, 1974

27. Swanson, Tatge, Natl. Bur. Stand. (U.S.), Circ. 539, 1 15 (1953)

28. A. Chamberod & J. Hillairet, Metallic Multilayers, Trans Tech Publications, 93, 1990

29. D. Tabor, J. Inst. Met. 79, 1(1951)

30. E. O. Hall, Nature, 173, 4411, May, 1954

31. William D. Callister, Jr., Materials Science and Engineering, third edition, John Wiley & Sons, Inc., 1994

32. Christopher M. A. Brett and Ana Maria Oliveira Brett, Electrochemistry – Principles, Methods and Applications, Oxford University Press, 1993

33. Multilayer Lab, a windows-application developed by the author of this thesis

34. M. F. Doerner and W. D. Nix, J. Mater. Res., 1, 4(1986)

35. W. C. Oliver and G. M. Pharr, J. Mater. Res., 7, 6(1992)

Vita Auctoris

Name:	Li Zhaojiang
Place of birth:	Gaomi County, Shandong Province, China
Education:	Beijing University, Beijing, China
	1982-1986, B. Sc.
	Beijing Institute of Labor Protection, Beijing, China
	1986-1990, M. Sc
	University of Windsor, Windsor, Ontario, Canada
	1997-1999, Master's candidate in physics